Supporting Information

Origin of Hydrocarbons Stability from a Computational Perspective: A Case Study of Ortho-Xylene Isomers

Mariusz P. Mitoraj,* Filip Sagan, Dariusz W. Szczepanik, Jurgens H. de Lange, Aleksandra L. Ptaszek, Daniel M. E. van Niekerk, and Ignacy Cukrowski*

Electronic Supplementary Information

PART 1

FAMSEC – theoretical background

Computational details

All structures were optimized in Gaussian 09 revision D.01 at the MP2/aug-cc-pVDZ level using keywords 'opt=verytight', 'int=ultrafine' and 'density=current'. AIMAll, ver. 16.10.31 was used for the QTAIM and IQA/Müller approximation calculations.

Basic and relevant to this work concepts of FAMSEC

The FAMSEC method[1] makes use of energy terms computed within the interacting quantum atoms (IQA)[2] molecular energy partitioning scheme that is the most powerful tool (at least among the Quantum Chemical Topology methods[3]) in the study of chemical bonds as well as inter- and intramolecular interactions on a fundamental level. Furthermore, IQF[4] (interacting quantum fragments) concepts are incorporated in the FAMSEC method and its usefulness in the study of intramolecular interactions and they role in explaining relative stability of conformers has been demonstrated recently.[5–7]

In IQA (as well as in FAMSEC) a molecular system is being considered as made of interacting with each other atoms that (i) fill in the entire space without voids in 3D molecular space or regions occupied by the system, (ii) do not overlap and (iii) are treated on equal footing regardless whether a classical chemist see atoms as covalently or otherwise (non)bonded. Hence, each atom A has well-defined interatomic boundaries and, as consequence, its own total or additive energy ($E_{\mathrm{add}}^{\mathrm{A}}$) such that electronic (or *ab initio*) molecular energy E, when partitioned into IQA-defined additive atomic energies, is recovered, $E = E_{\mathrm{IQA}}$, where

$$E_{\mathrm{IQA}} = \sum_{\mathrm{A}} E_{\mathrm{add}}^{\mathrm{A}} \qquad (1)$$

It is important to realize that $E_{\mathrm{add}}^{\mathrm{A}}$ depends mainly on the kind of an atom and, to a lesser degree, on its placement in a molecule. This is the placement of an atom in a molecule that has an impact

on self-atomic energy ($E_{\text{self}}^{\text{A}}$) and the kind, nature as well as strength of an interaction atom A is involved in with another atom of the system ($E_{\text{int}}^{\text{A,B}}$). When a molecular system undergoes a change from any initial state (reference, *ref* state) to another state (treated as final, *fin* state) on, *e.g.* conformational transformation, then $E_{\text{IQA}}(fin) \neq E_{\text{IQA}}(ref)$ due to changes in the IQA energy components. It is then clear that one should be able to pin-point the main origin of $\Delta E = \Delta E_{\text{IQA}} = E_{\text{IQA}}(fin) - E_{\text{IQA}}(ref)$ from analyses of changes in the IQA- and FAMSEC-defined energy terms.

The concept of FAMSEC stems from the need to understand and explain (in terms of classical thinking) changes taking place throughout a molecule in a new environment. FAMSEC is focused on providing qualitative and quantitative answers to two typical and of fundamental significance questions a chemist might ask related to the *ref* → *fin* change:

1. What is the impact on properties (and related to it energetic effects) of a selected (on purpose) and chemically meaningful *n*-atom fragment $\mathcal{G}$ of a system? This implies changes in properties confined only to a 3D space occupied by $\mathcal{G}$ and *loc*-FAMSEC energy term applies

   $$loc\text{-FAMSEC} = \Delta E_{\text{self}}^{\mathcal{G}} + \Delta E_{\text{int}}^{\mathcal{G}} \quad (2)$$

   The $\Delta E_{\text{self}}^{\mathcal{G}}$ term accounts for self-fragment energy change, i.e., a sum of self-atomic energy changes of atoms constituting a molecular fragment $\mathcal{G}$. The $\Delta E_{\text{int}}^{\mathcal{G}}$ term quantifies the intrafragment interaction energy change and when $\mathcal{G}$ is made of two atoms it quantifies a diatomic interaction energy change. From this follows that *loc*-FAMSEC might be useful in identifying parts of a molecule that experienced most significant decrease (or increase) of their energies that can be interpreted as being most stabilised (or strained, respectively) in *fin* relative to *ref*.
2. When in *fin*, has the fragment of interest $\mathcal{G}$ stabilised (or otherwise) the entire molecule? To address this, the remaining atoms of a molecule are considered as another molecular fragment $\mathcal{H}$ and a quantified answer is provided by the *mol*-FAMSEC energy term,

$$mol\text{-FAMSEC} = loc\text{-FAMSEC} + \Delta E_{\text{int}}^{\mathcal{GH}} \quad (3)$$

where the $\Delta E_{\text{int}}^{\mathcal{GH}}$ energy term quantifies the interfragment interaction energy change. Moreover, when $\Delta E_{\text{int}}^{\mathcal{GH}} < 0$ then it implies that, relative to *ref* state, $\mathcal{G}$ found itself in more attractive (stabilizing) molecular environment when in the *fin* state. The interplay between the two components, *loc*-FAMSEC and $\Delta E_{\text{int}}^{\mathcal{GH}}$, decides whether the molecular fragment $\mathcal{G}$ has added to stability of the *fin* state of a molecular system (then *mol*-FAMSEC < 0) or contributed in a destabilizing manner. Furthermore, one can also compute the $\Delta E_{\text{int}}^{\mathcal{GH}}$ term from

$$\Delta E_{\text{int}}^{\mathcal{GH}} = \Delta \sum_{\text{X}\neq\text{A}} E_{\text{int}}^{\text{A,X}} + \Delta \sum_{\text{X}\neq\text{B}} E_{\text{int}}^{\text{B,X}} - 2\,\Delta E_{\text{int}}^{\mathcal{G}} \quad (4)$$

where, for simplicity, a two-atom fragment $\mathcal{G}$ = {A,B} is considered. The first two terms describe how the sum of interactions between an atom A (or B) belonging to $\mathcal{G}$ and each other atom X in a molecule changed on *ref* $\rightarrow$ *fin*. From that one can gain an insight on how (un)favourably the molecular environment changed in relation to each atom of the $\mathcal{G}$ fragment.

It is important to stress that the *loc*- and *mol*-FAMSEC terms can be computed for all unique, 2-, 3-, … *n*-atom, fragments. From that one can establish which fragments were most locally (de)stabilized and which ones (de)stabilized a molecule most, *etc.* This is very useful information in interpreting many chemical phenomena and also puts the energies attributed to a selected fragment in molecular-scale perspective.

Finally, it has been shown in the recent study of relative stability of glycol conformers[7] that the FAMSEC data obtained at the MP2 level using the Müller approximation in the IQA calculations (the MP2/ Müller combination was also used in this work) closely approach values obtained at the exceptionally well performing CCSD/BBC1 combination.

Interpretation of the selected FAMSEC data.

For the purpose of the present studies that is focused on relative stability of two xylene conformers (*in-in* and *out-out*) it is important to understand the impact of bi-directional (rather than unidirectional) structural transformation, expressed as *in-in* ↔ *out-out*, on the properties of atoms and chemically meaningful molecular *n*-atom fragments ($n \geq 2$). The advantage of bi-directional approach is in that it facilitates interpretation of and visualising computed changes using relevant structures. To ease interpretation, molecular fragments will be marked on molecular graphs of either the *in-in* (or *out-out*) conformer representing the *fin* state of a structural change. A blue-coloured solid-line and red-coloured dashed-line rectangles will be used throughout to indicate, respectively, changes of stabilizing and destabilizing nature in the fragment's computed property. In addition, the computed value, in kcal/mol, will also be placed on the molecular graph for each marked fragment. To this effect, it is important to note that the computed change in, *e.g.*, the diatomic interaction energy, $\Delta E_{\text{int}}^{\text{A,B}}$, for *in-in* → *out-out* is exactly the same in absolute values but with an opposite sign as that obtained for *out-out* → *in-in* (the same applies to all FAMSEC energy terms discussed in this work).

Insight from changes in additive atomic energies. Changes in additive atomic energies computed for individual atoms are shown in Fig. 1.1; this can be seen as a kind of topology of $\Delta E_{\text{add}}^{\text{A}}$ distribution throughout a molecule in the *fin* structure, either *in-in* (from the *out-out* → *in-in* transformation) or *out-out* (from the *in-in* → *out-out* transformation).

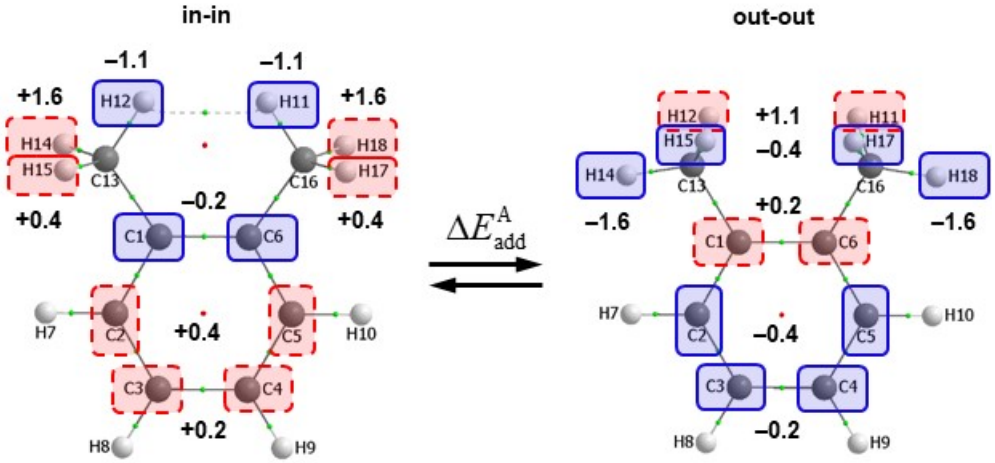

Figure 1.1. Topology of changes in additive atomic energies computed for individual atoms on *in-in* ↔ *out-out* structural changes of xylene. Atoms stabilized are marked by blue coloured solid-line rectangles and destabilised atoms are marked by red coloured dashed-line rectangles. All values are in kcal/mol.

Possibly unexpectedly, H11 (H12) became most stabilised in *in-in* among all atoms, by –1.1 kcal/mol that is 5-times more significant than –0.2 kcal/mol computed for C1 (C6). Obviously, H11/H12 became most destabilised on the *in-in* → *out-out* structural change, by +1.1 kcal/mol. All remaining atoms became destabilised in *in-in* but totally unpredictably, H14 (H18) top the list with $\Delta E^{H14}_{add} = +1.6$ kcal/mol that is (i) 4-times more than any other destabilised atom and (ii) larger, in absolute value, than stabilization experienced by H11 (H12). On the *in-in* → *out-out* change, H14 (H18) became most stabilised and by looking at the *out-out* structure, this must be linked with the 'open'-ring formation; we call it open because there is no atomic interaction line (typically called a bond path) between H7 and H14.

Trends in Fig.1.1 clearly show that:

1. The aromatic ring does not 'like' the competition posed by the formation of 6-membered 'closed'-ring with an atomic interaction line (AIL, commonly called a bond path)) linking atoms involved in the steric contact H11--H12; note that four out of six aromatic carbons became destabilised in *in-in*.
2. The formation of the stabilised 6-membered ring in *in-in* can be seen as (C-C)-assisted; note that the atoms C1–C6, constituting the link (foundation or base) of the bay (6-membered ring), are the only C-atoms that became stabilised in *in-in*.
3. It appears that formation of either 'open' or 'closed' in-plane rings is structurally favoured. Notably, 6-membered 'closed'-ring in *in-in* and 5-membered 'open'-ring in *out-out* are in plane with the aromatic ring in both structures.

Table 1.1. Changes in additive atomic energies (in kcal/mol) computed for the indicated structural changes of xylene.

	ΔE^{A}_{add}		
Atom	**From out-out to in-out**	**From in-out to in-in**	**From out-out to in-in**
C1	0.1	-0.3	-0.2
C2	0.1	0.3	0.4
C3	0.2	0.0	0.2
C4	0.0	0.2	0.2
C5	0.3	0.2	0.4
C6	-0.3	0.1	-0.2
H7	0.0	0.0	0.0
H8	0.0	0.0	0.0
H9	0.0	0.0	0.0
H10	0.0	0.0	0.0
H11	0.0	-1.1	-1.1
H12	-1.1	0.0	-1.1
C13	-0.7	0.7	0.0
H14	1.6	0.0	1.6
H15	0.5	0.0	0.4
C16	0.5	-0.5	0.0
H17	0.0	0.4	0.4
H18	0.0	1.6	1.6

An n-atom molecular fragment $\mathcal{G}$ based analysis of $\Delta E^{\mathcal{G}}_{\text{add}}$ is depicted in Fig. 1.2.

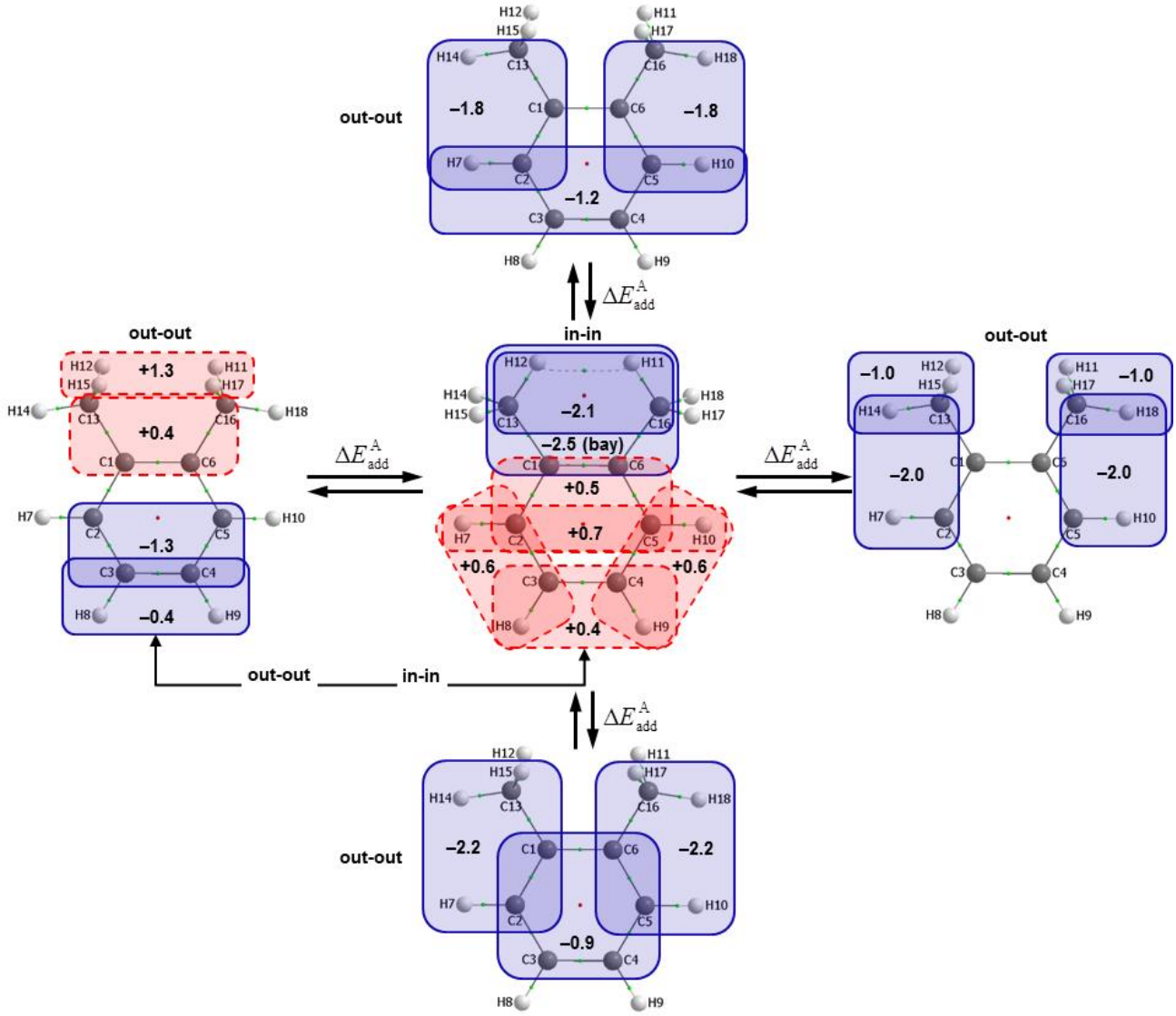

Figure 1.2. Topology of changes in additive fragment energies (as a sum of additive atomic energies) computed for the indicated 4-, 5- and 6-atom molecular fragments on *in-in* ↔ *out-out* structural changes of xylene. Fragments stabilized are marked by blue coloured solid-line rectangles and destabilised fragments are marked by red coloured dashed-line rectangles. All values are in kcal/mol.

Although it is self-explanatory, it is important to point at a few important observations:

A) This is the entire bay (in plane with the aromatic ring in *in-in*) that became stabilised. All other (4–6)-atom fragments became destabilised on the *out-out* → *in-in* transformation. To ease an interpretation, let us give two examples:

(i) A 4-atom fragment {C1,C2,C5,C6} is marked in *in-in* by a red-coloured dashed-line rectangle indicating that it was destabilised on *out-out* → *in-in* (there are also other two 4-atom destabilised fragments shown on the molecular graph of the *in-in* structure).

(ii) Two 6-atom fragments (the aromatic ring and the {C1,C2,H7,H14,H15,C13} overlapping fragment) became stabilised in *out-out* by –0.9 and –2.2 kcal/mol, respectively. This means that the same fragments become destabilised when the *out-out* changes to *in-in*.

B) Indeed, the aromatic ring became stabilised in *out-out* but surprisingly much less than:

(i) The 'closed'-ring in *in-in* ($\Delta E^{\mathcal{G}}_{\text{add}}$ = –2.5 kcal/mol)

(ii) The 'open'-ring in *out-out* ($\Delta E^{\mathcal{G}}_{\text{add}}$ = –2.2 kcal/mol)

Insight from the loc-FAMSEC energy term. Let us start with smallest fragments as 2-atom-based approach is solidly entrenched in classical thinking and interpretation of chemical bonding as well as intramolecular interactions/clashes – relevant data is shown in Figure 1.3. One must recall that the *loc*-FAMSEC terms is perfectly suited to identify potentially strained (destabilized) fragments of a molecule due to accounting for both self-deformation of atoms constituting a fragment and interatomic interactions. Focusing on the *in-in* conformer (middle part in Fig. 1.3) we note that all possible 2-atom fragments of the bay made of covalently bonded atoms as well as $\mathcal{G}$ = {H11,H12} are not strained as *loc*-FAMSEC < 0 is observed for all of them.

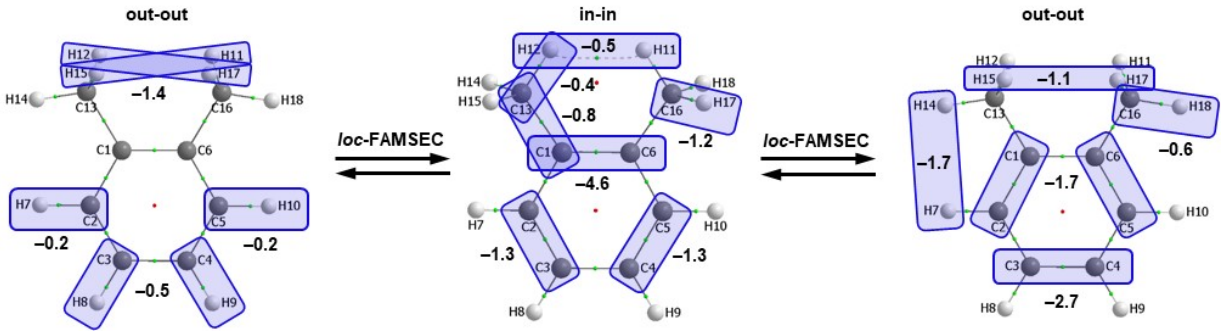

Figure 1.3. Topology of *loc*-FAMSEC energy terms computed for the indicated 2-atom fragments on *in-in* ↔ *out-out* structural changes of xylene. All values are in kcal/mol.

Similarly, the bay–type {H12,H17}/{H11,H15} and side–type {H7,H14}/{H10,H18} in *out- out* are locally stabilized by –1.4 kcal/mol and –1.7 kcal/mol, respectively, Fig. 1.3. It is now important to compare contributions leading to stabilisation of the {H11,H12} in *in-in* and {H7,H14} in *out-out*. We found that diatomic interaction energy changed in stabilising manner with $\Delta E_{\text{int}}^{\mathcal{G}}$ of –3.5 and –1.1 kcal/mol for {H11,H12} in *in-in* and {H7,H14} in *out-out*, respectively. However, the trend in $\Delta E_{\text{self}}^{\mathcal{G}}$ is different for the two fragments, self-fragment energy of {H11,H12} increased by +3.0 kcal/mol whereas it decreased in the case of {H7,H14} by –0.6 kcal/mol; recall that the sum of these energy changes, $\Delta E_{\text{int}}^{\mathcal{G}}$ and $\Delta E_{\text{self}}^{\mathcal{G}}$, makes up the *loc*-FAMSEC term and in both cases *loc*-FAMSEC < 0 was obtained.

Interestingly, the trend found for the {H11,H12} fragment in *in-in*, i.e., $\Delta E_{\text{self}}^{\mathcal{G}} > 0$, $\Delta E_{\text{int}}^{\mathcal{G}} < 0$ and $\left|\Delta E_{\text{int}}^{\mathcal{G}}\right| > \left|\Delta E_{\text{self}}^{\mathcal{G}}\right|$, was also found for atoms directly involved in the intramolecular classical H-bonding (with an AIL present) in the protonated ethylenediamine, protonated ethanolamine and β-alanine as well as in the lowest energy conformer of glycol without AIL between the interacting O and H atoms.[1] An interesting pattern is observed among C-atoms of the aromatic ring in the *in-in* conformer – every second atom-pair became locally stabilised with the {C1,C6} fragment (it constitutes the base of the bay) being stabilised most with *loc*-FAMSEC = –4.6 kcal/mol. Complementary, also every second 2-atom fragment of the aromatic ring in the *out-out* conformer became stabilised but not as much as {C1,C6}; note that for most stabilised {C3,C4} we obtained *loc*-FAMSEC of –2.7 kcal/mol. It is fully consistent with the bond distances, Nalewajski-Mrozek bond orders as well as the calculated one-bond NMR spin-spin coupling constants shown in ESI (part 2, Table 2.1).

Data computed for larger molecular fragments is shown in Figure 1.4.

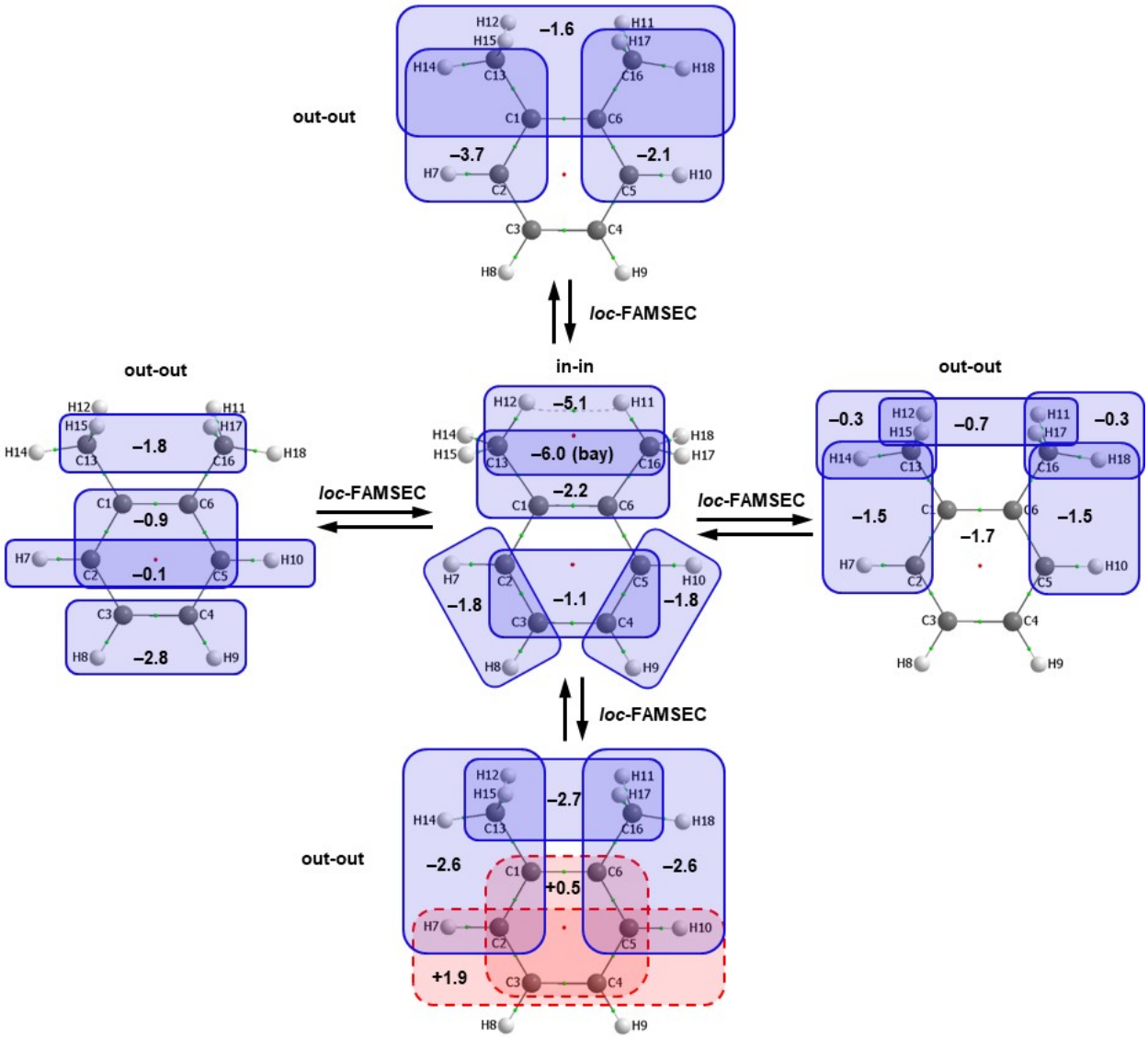

Figure 1.4. Topology of *loc*-FAMSEC energy terms computed for the indicated *n*-atom fragments on the *in-in* ↔ *out-out* structural changes of xylene. Fragments stabilized are marked by blue-coloured solid-line rectangles and destabilised fragments are marked by red-coloured dashed-line rectangles.All values are in kcal/mol.

Insight from the mol-FAMSEC energy term. Data shown in Figure 1.5 (part A) demonstrates that the bay {H11,H12} fragment, containing atoms involved in 'a classical steric clash', has contributed in a stabilising manner to the *in-in* conformer's energy: *mol*-FAMSEC of –3.8 kcal/mol was obtained.

Part A.

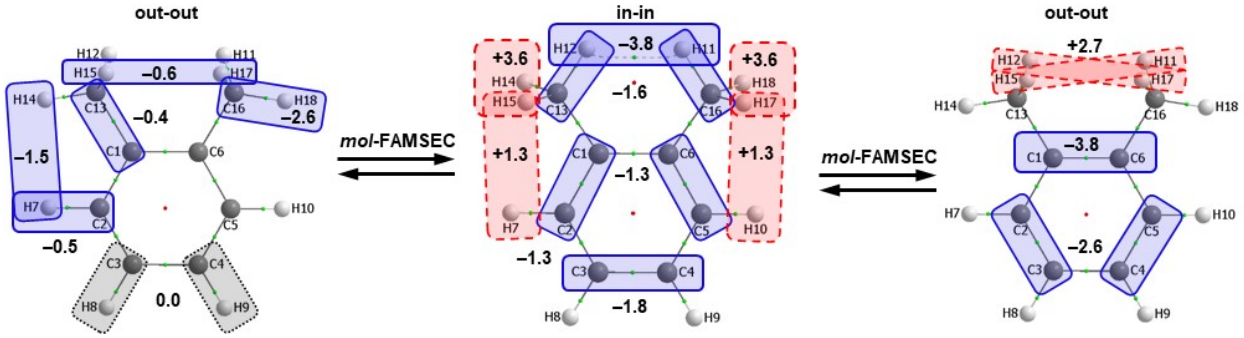

Part B.

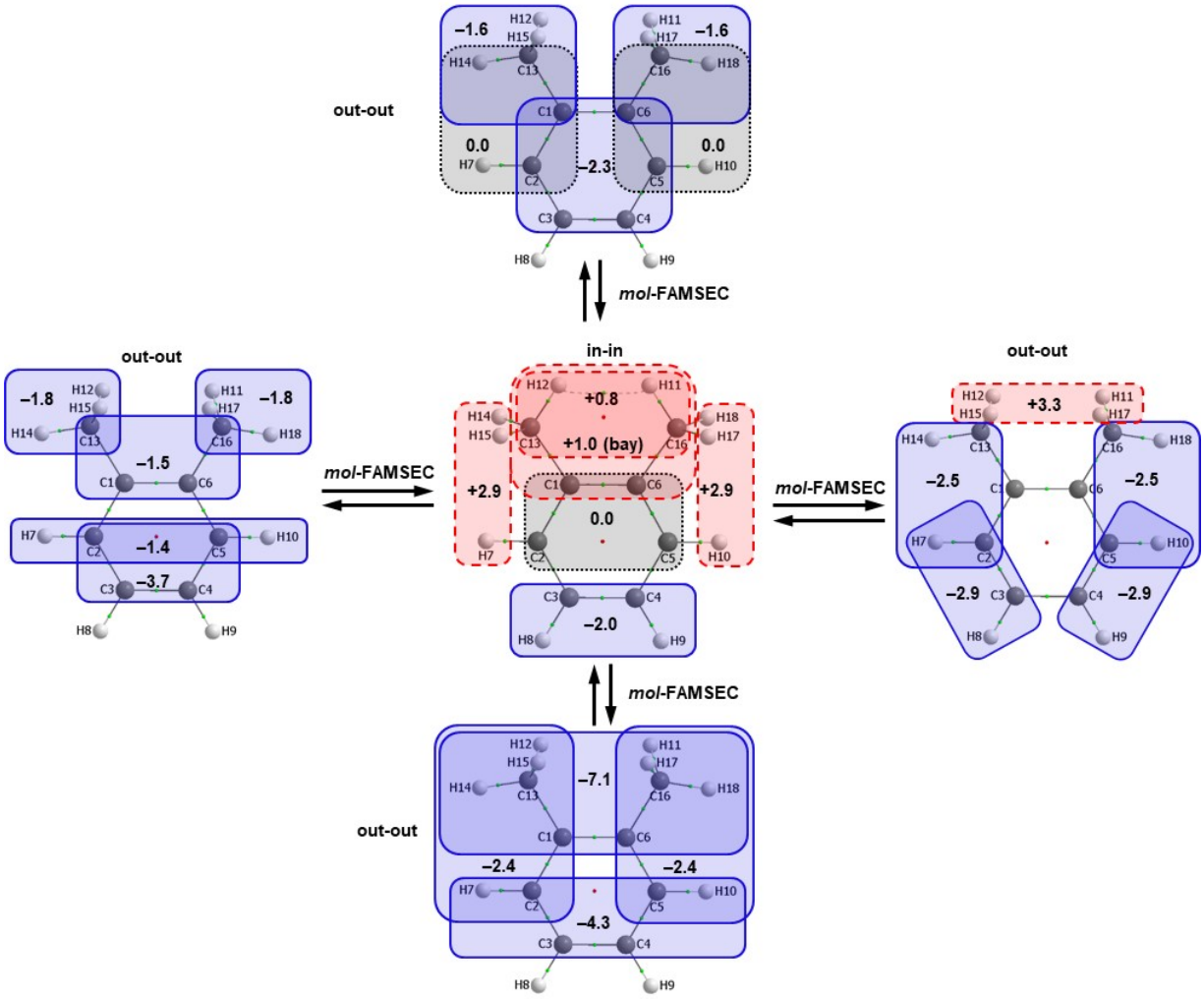

Figure 1.5. Topology of *mol*-FAMSEC energy terms computed for the indicated 2-atom (Part A) and *n*-atom fragments (Part B) on the *in-in* ↔ *out-out* structural changes of xylene. Fragments stabilized are marked by blue-coloured solid-line rectangles and destabilised fragments are marked by red-coloured dashed-line rectangles. Fragments that had insignificant contribution to molecular stability are marked by black-coloured dotted-line rectangles. All values are in kcal/mol.

Also three C–C fragments of the aromatic ring added to the in-in stability but significantly less, among them {C3,C4} contributed most significantly with mol-FAMSEC of –1.8 kcal/mol. Among 2-atom fragments that destabilised *in-in* most are {H14,H15}/{H17,H18} with *mol*-FAMSEC of +3.6 kcal/mol and {H7,H15}/{H10,H17} with *mol*-FAMSEC of +1.3 kcal/mol. The bay-type {H17,H15} and side-type {H14,H7} interactions stabilize *out-out* conformation. It is notable to add that London dispersion forces are a crucial component of intramolecular dihydrogen bonding C–H···H–C in addition to charge delocalization contribution as demonstrated for 2-butene isomers.[5] The importance of the latter term in other untypical anion-π interactions has been also recognized.[8] To further reference, an excellent reviews on homopolar dihydrogen contacts in hydrogen storage materials are available in Ref. [9-11].

Even more insightful data that correlates very well with classical thinking is obtained for larger fragments shown in Figure 1.5 (part B). First of all, the entire aromatic ring stabilised *out-out* (*mol*-FAMSEC = –2.3 kcal/mol) isomer which is in accord with the conclusions stemming from the EDDB, HOMA and NICS descriptors (Table 1). Importantly, there are other fragments that stabilised *out-out* significantly more; it appears that the entire 'top' part of *out-out* (the 10-atom fragment containing MeC=CMe units) can be seen as mainly responsible for higher stability of the *out-out* conformer (*mol*-FAMSEC = –7.1kcal/mol). Clearly, more efficient hyperconjugation effects and consequently more pronounced interactions of the methyl units with the phenyl rings (as indicated by ETS-NOCV) results in the superior stabilisation of the entire top MeC=CMe fragment in *out-out* vs. *in-in*, Figure 1.5 (part B). Interestingly, the entire bay as well as the C–H···H–C fragment of the bay slightly destabilised the *in-in* conformer with the *mol*-FAMSEC of +1.0 and +0.8 kcal/mol, respectively. Furthermore, this is the 4-atom fragment of the bay that is made of C-atoms, {C13,C1,C6,C16}, that destabilised more *in-in* with *mol*-FAMSEC = +1.5 kcal/mol – this fragment, for clarity, is marked on the *out-out* structure (with the opposite *mol*-FAMSEC = –1.5 kcal/mol). This result clearly indicates the loss of hyper-conjugation on the *out-*

out → *in-in* change, given the *loc*-FAMSEC results above, as well as results from the other methods used in this work. However, *in-in* was destabilised most by two equivalent 3-atom fragments, among them {H7,H14,H15} for which *mol*-FAMSEC of +2.9 kcal/mol was obtained. Finally, the 'bottom' of the aromatic ring, *i.e.*, the 4-atom {H8,C3,C4,H9} fragment is the only meaningful fragment that stabilised *in-in*; note that there are many *n*-atom fragments (n ≥ 4) that stabilised *out-out*, hence they made a destabilising contribution on the *out-out* → *in-in* change.

References

1. I. Cukrowski, *Comput. Theor. Chem.*, 2015, **1066**, 62–75.
2. M. A. Blanco, A. M. Pendás and E. Francisco, *J. Chem. Theory Comput.*, 2005, **1**, 1096–1109.
3. N. O. J. Malcolm and P. L. A. Popelier, *Faraday Discuss.*, 2003, **124**, 353–363.
4. A. M. Pendás, E. Francisco and M. A. Blanco, *Faraday Discuss*., 2007, **135**, 423–438.
5. I. Cukrowski, F. Sagan and M. P. Mitoraj, *J. Comp. Chem.*, 2016, **37**, 2783–2798.
6. I. Cukrowski, D. M. E. van Niekerk and J. H. de Lange, *Struct. Chem.*, 2017, **28**, 1429–1444.
7. I. Cukrowski and P. M. Polestshuk, *Phys. Chem. Chem. Phys.*, 2017, **19**, 16375–16386.
8. Y.P. Yurenko, S. Bazzi, R. Marek J. Kozelka *Chem. Eur. J.* 2017,**23**, 3246.
9. D. J. Wolstenholme, J. L. Dobson, G. S. McGrady, *Dalton Trans.* **2015**, *44*, 9718
10. D.J. Wolstenholme, K.T. Traboulsee, Y. Hua, L.A. Calhoun, G.S. McGrady *ChemComm* 2012, **48**, 2597
11. D.J. Wolstenholme, E.J. Fradsham, G.S. McGrady *CrystEngComm*, 2015, **17**, 7623.

PART 2 – ETS-NOCV and DAFH

Table 2.1. Selected changes in bonds parameters (out-out→in-in) expressed by distances, Nalewajski-Mrozek bond orders, IQA/FAMSEC interaction energies and one-bond NMR spin-spin coupling constants.

Bond	Δd(MP2) [Å]	Δd(CCSD) [Å]	ΔBO [a.u]	ΔE_{int} [kcal/mol]	$\Delta E_{attr-loc}$ [kcal/mol]	*Δ|J| [Hz]
C1-C6	-0.0014	-0.0050	+0.0345	-2.18	-4.60	+4.468
C1-C2	+0.0058	+0.0091	-0.0308	+2.52	+1.73	-2.509
C2-C3	-0.0044	-0.0075	+0.0330	-2.16	-1.29	+1.725
C3-C4	+0.0020	+0.0054	-0.0304	+1.78	+2.67	-1.413
C4-C5	-0.0044	-0.0075	+0.0330	-2.16	-1.29	+1.725
C5-C6	+0.0058	+0.0091	-0.0308	+2.52	+1.73	-2.509
C1-C13	+0.0054	+0.0050	-0.0061	+1.15	-0.79	+0.061
C6-C16	+0.0054	+0.0050	-0.0061	+1.15	-0.79	+0.061
H11-H12	-0.5130	-0.5192	-	-3.49	-0.49	+2.007
H7-H14	+0.3264	+0.3279	-	+1.08	+1.70	+0.309

* Absolute values of J are taken into consideration, due to H-H couplings being negative.

As one can notice from Table 2.1, all parameters match and support each other in the conclusion that the bonds of phenyl ring C1-C6, C2-C3 and C4-C5 are strengthening and C1-C2, C3-C4, C5-C6 connections are weakening during the out-out to in-in rotation. Correspondingly, the calculated NMR spin-spin coupling constants rise for the strengthened bonds and drop for the weakened connections. As far as the CH···HC contacts are concerned, the H11-H12 interactions matches in its description more classical C-C bonds that are strengthened, indicating a stabilization upon closing the distance between atoms.

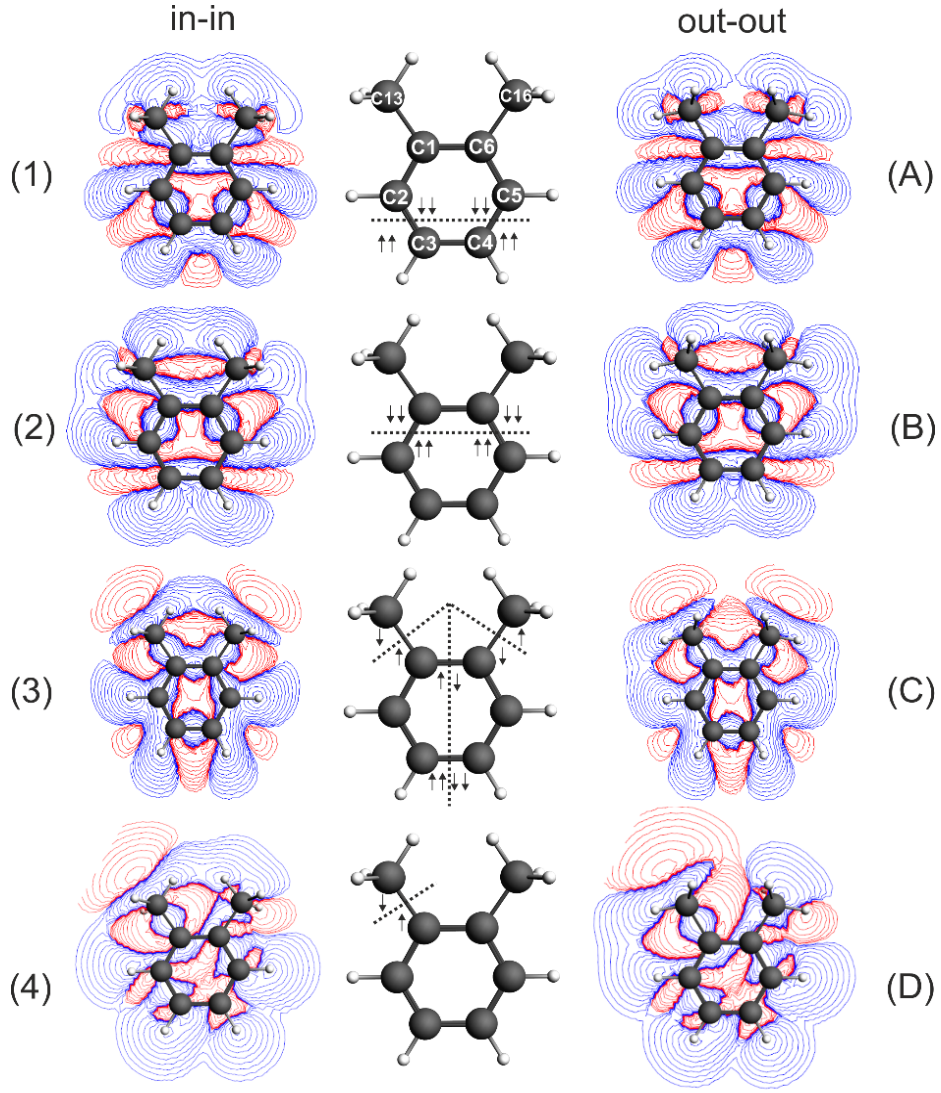

Fig. 2.1. Partitionings of the xylene molecules considered in ETS-NOCV calculations. Arrows denote spin of unpaired electrons due to the bond cleavage. On sides, maps of $\Delta\rho_{total}$ in the plane of aromatic ring.

To describe bonding within the system from ETS-NOCV perspective, several fragmentations were considered: (**1**) $C_2H_2{\uparrow}{\uparrow}{\uparrow}{\uparrow}|{\downarrow}{\downarrow}{\downarrow}{\downarrow}C_6H_8$ two quintet fragments created by cleavage of C2-C3 and C4-C5 bonds, (**2**) $C_4H_4{\uparrow}{\uparrow}{\uparrow}{\uparrow}|{\downarrow}{\downarrow}{\downarrow}{\downarrow}C_4H_6$ two quintet fragments created by cleavage of C1-C2 and C5-C6 bonds, (**3**) $CH_3{\uparrow}|CH_3{\downarrow}|C_3H_2{\uparrow}{\uparrow}{\uparrow}{\uparrow}|{\downarrow}{\downarrow}{\downarrow}{\downarrow}C_3H_2$ four fragment division created by cleavage of C1-C6 and C3-C4 bonds and separating methyl groups and finally (**4**) two fragments created by separating singular methyl group $CH_3{\uparrow}|{\downarrow}C_6H_7$, as shown on Fig. 2.1. Such fragmentations can be used to extract information about cleaved bonds and interactions between methyl groups in both conformers.

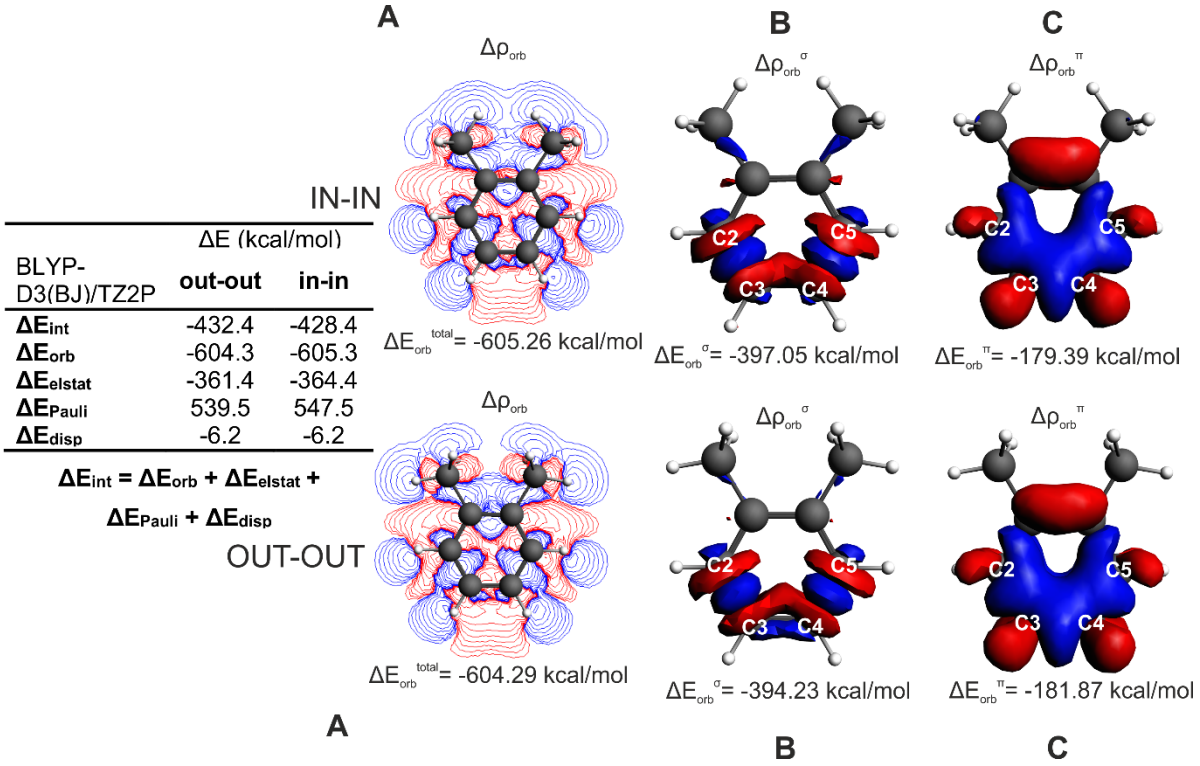

Fig. 2.2. Fragmentation **1** summary: energy decomposition together with $\Delta\rho_{orb}$ maps in the plane of aromatic ring (A). σ (B) and π (C) components of $\Delta\rho_{orb}$.

Comparing energies of orbital interaction between fragments ($\Delta\rho_{orb}$) of two conformers is an another way of deducing their strength. Orbital stabilization upon combining the fragments in fragmentation **1**, suggests the strengthening of the cleaved bonds – C2-C3 and C4-C5 when the out-out → in-in rotation is considered, Fig. 2.2. Decomposition of differential electron density into σ and π components reveals that the source of the difference in interaction energies is a varying stabilization provided by σ bonds, Fig. 2.2. Interestingly, π component is more stabilizing in out-out conformation.

IN-IN

BLYP-D3(BJ)/TZ2P	ΔE (kcal/mol) out-out	in-in
ΔE_{int}	-419.3	-421.7
ΔE_{orb}	-612.6	-610.4
ΔE_{elstat}	-380.4	-378.4
ΔE_{Pauli}	581.8	575.3
ΔE_{disp}	-8.1	-8.2

$\Delta E_{int} = \Delta E_{orb} + \Delta E_{elstat} + \Delta E_{Pauli} + \Delta E_{disp}$

OUT-OUT

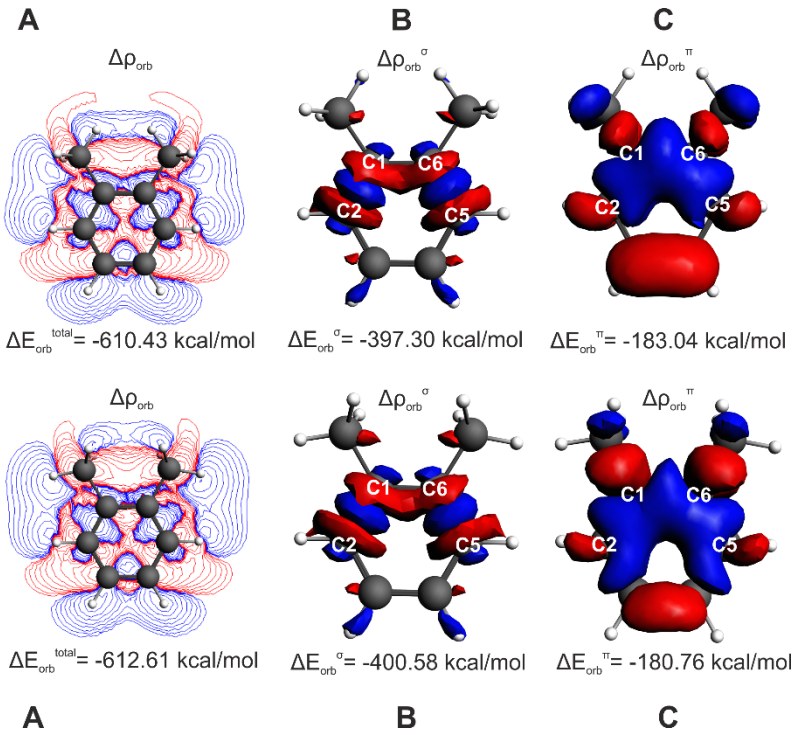

Fig. 2.3. Fragmentation **2** summary: energy decomposition together with $\Delta\rho_{orb}$ maps in the plane of aromatic ring (A). σ (B) and π (C) components of $\Delta\rho_{orb}$.

Accordingly, the same analysis can be made for fragmentation **2**. Here, information about bonds C1-C2 and C5-C6 can be extracted. ΔE_{orb} is clearly lower for the out-out conformer, supporting the notion that these bonds are weakening in the out-out → in-in rotation, Fig.2.3. Decomposition into σ and π components shows similar trends as in the fragmentation **1**, namely, energy difference is caused by more pronounced stabilization of σ bonds in the out-out xylene, and is partially offseted by opposite energetics of the π bond, Fig.2.3.

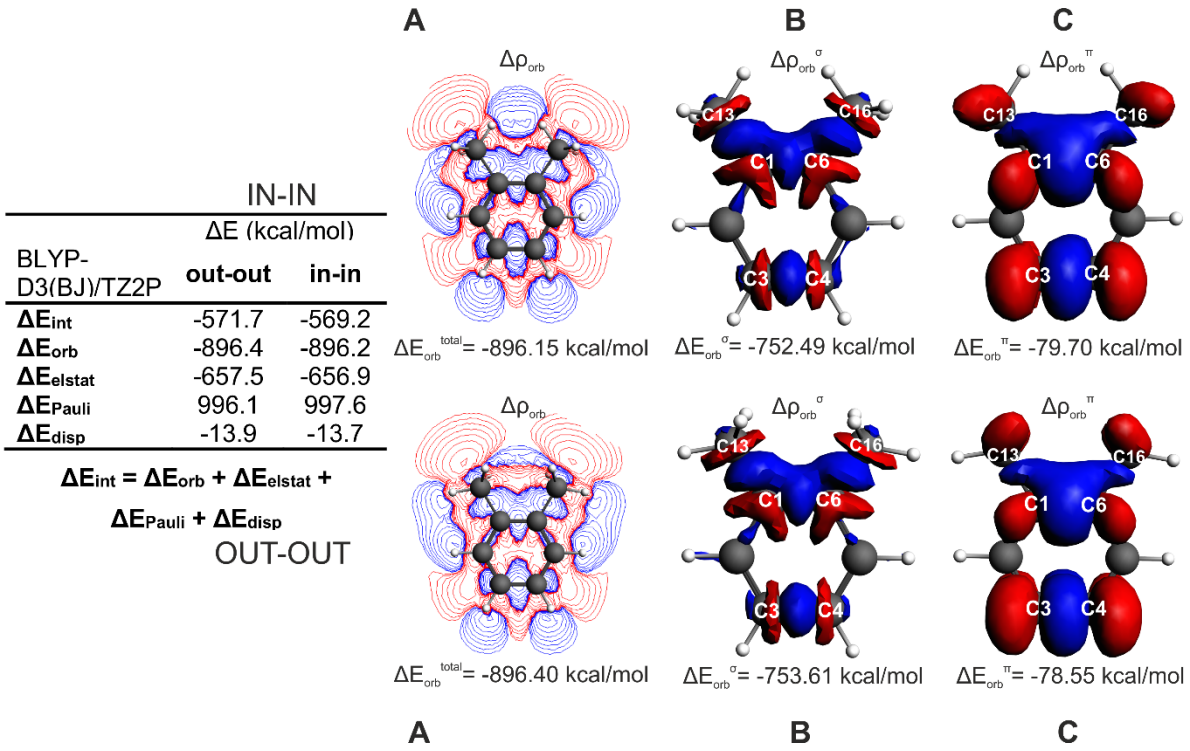

Fig. 2.4. Fragmentation **3** summary: energy decomposition together with $\Delta\rho_{orb}$ maps in the plane of aromatic ring (A). σ (B) and π (C) components of $\Delta\rho_{orb}$.

Orbital interaction energies (ΔE_{orb}) of both conformers are very similar in the fragmentation **3**, Fig.2.4. It is due to the fact that some of the cleaved bonds (C1-C6, C1-C13, C6-C16) are stabilizing in the considered rotation while the others are destabilized (C3-C4), resulting in no significant net change in energy.

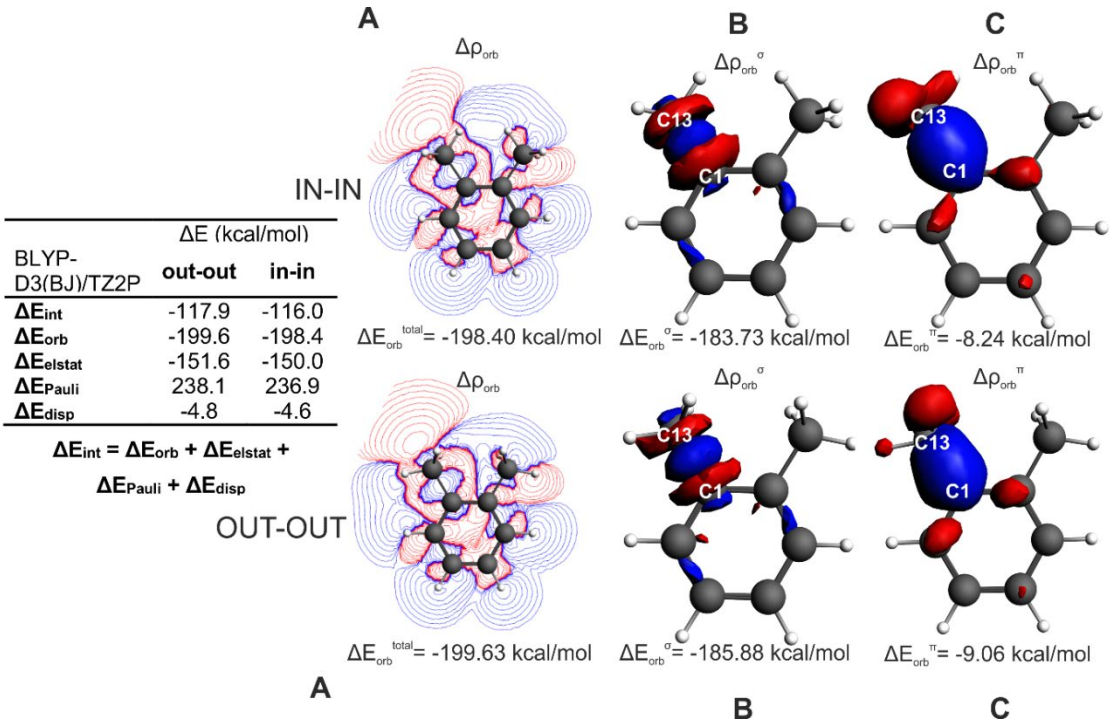

Fig. 2.5. Fragmentation **4** summary: energy decomposition together with $\Delta\rho_{orb}$ maps in the plane of aromatic ring (A). σ (B) and π (C) components of $\Delta\rho_{orb}$.

In line with the bond order analysis, information provided by fragmentation **4** suggest that C1-C13 bond is weakening in the out-out -> in-in rotation. Both σ and, interestingly, π components are weakened, Fig 2.5.

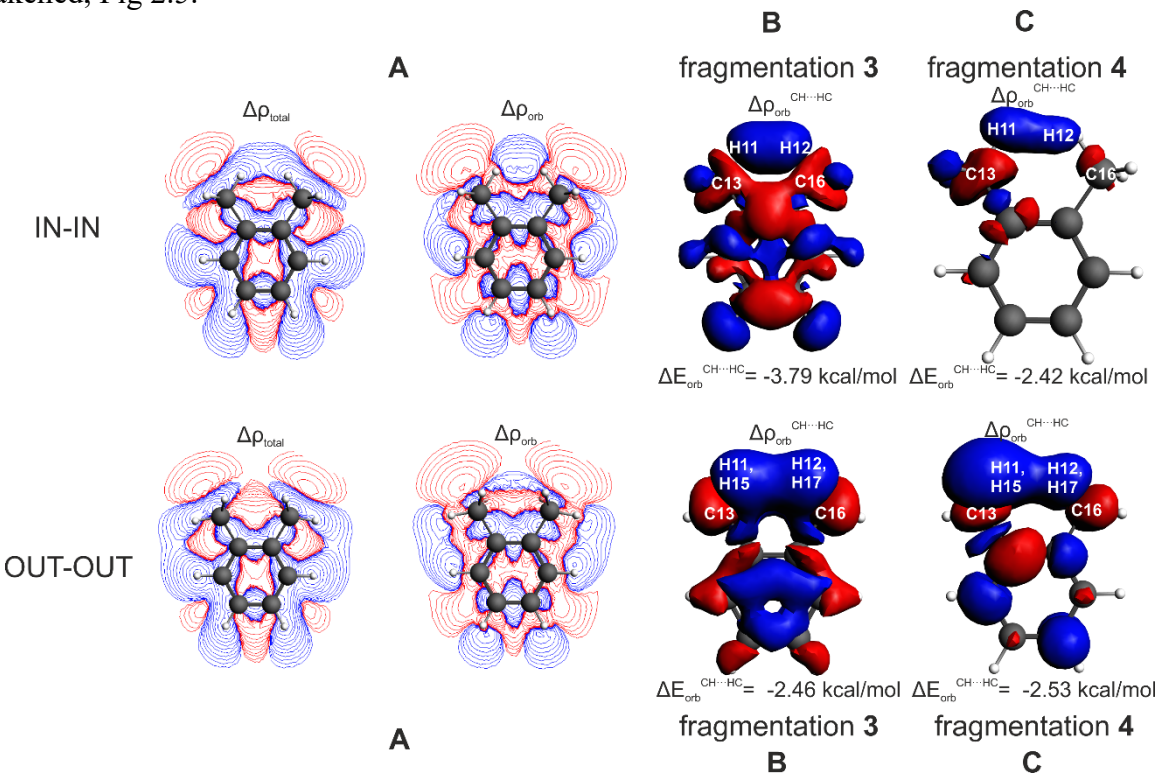

Fig. 2.6. CH···HC interactions between methyl groups as captured by fragmentations **3** and **4**.

Fragmentation **3** has been chosen for extracting interactions between the hydrogen atoms in methyl groups. Such interactions were captured both in the in-in and the out-out xylene, Fig 2.6., confirming FAMSEC-based findings. Although C-H···H-C interactions are not fully isolated, it seems that their energetics is consistent between methods – single interaction in the in-in conformer is stronger than the two contacts in the out-out. It should be pointed out that in the in-in xylene, said interaction is visible on both $\Delta\rho_{orb}$ and $\Delta\rho_{total}$ cut planes, Fig 2.6. Fragmentation **4** provides better isolated image of C-H···H-C interaction in the in-in xylene, but in the out-out conformer, a significant π component from the aromatic ring is present, rendering the energetic comparison invalid, Fig 2.6.

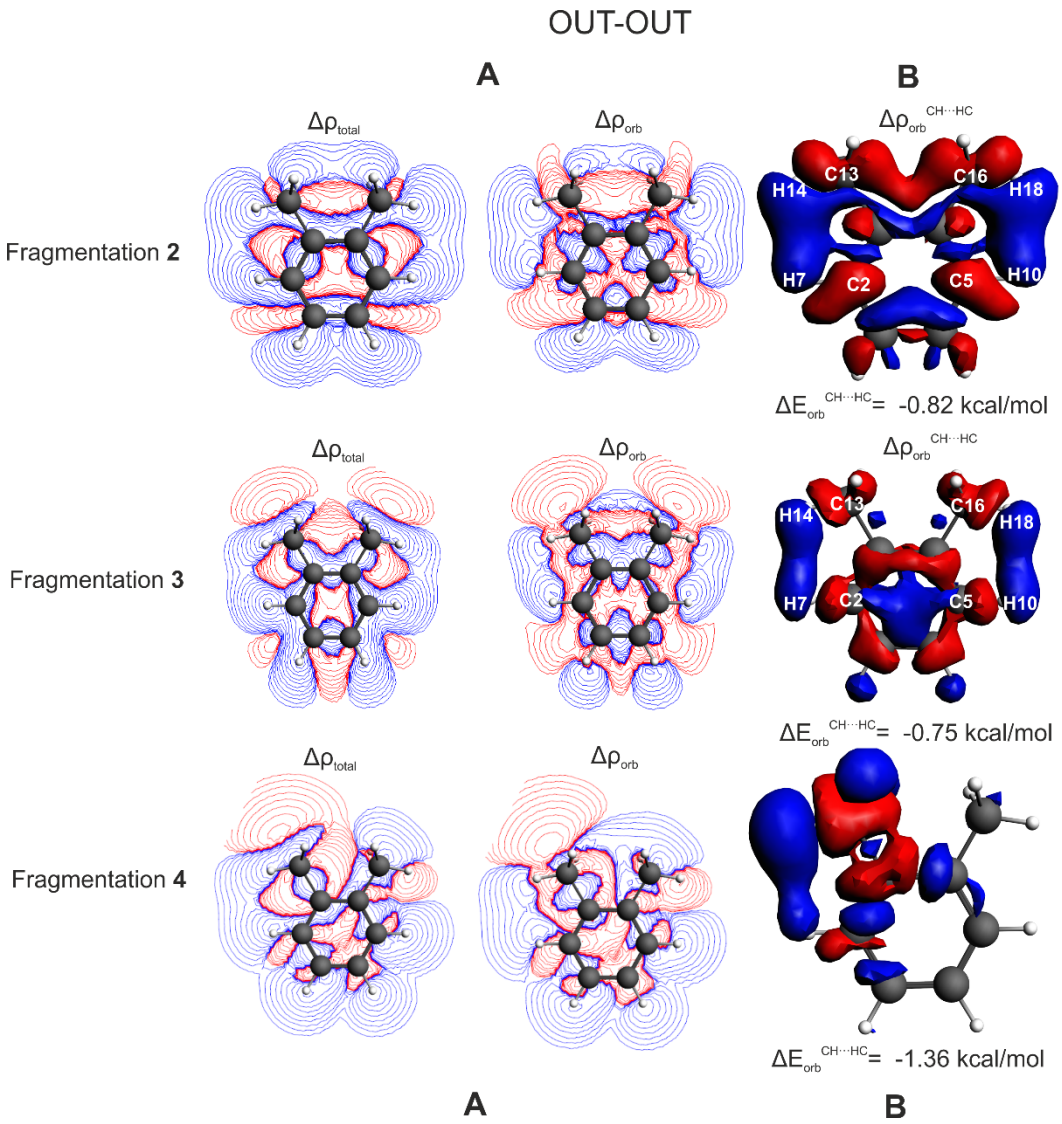

Fig. 2.7. CH···HC interactions between methyl groups and H7 and H10 atoms from aromatic ring, as captured by fragmentations **2**, **3** and **4**.

Analyzing cut plane of $\Delta\rho_{orb}$ of the out-out xylene, one can find an accumulation of electron density between hydrogen atoms H7···H14 and H10···H18. Corresponding NOCVs also can be found, Fig.2.7. Fragmentations **2** and **3** 'cuts' these interactions as well and, as it turns out, similar NOCVs are present.

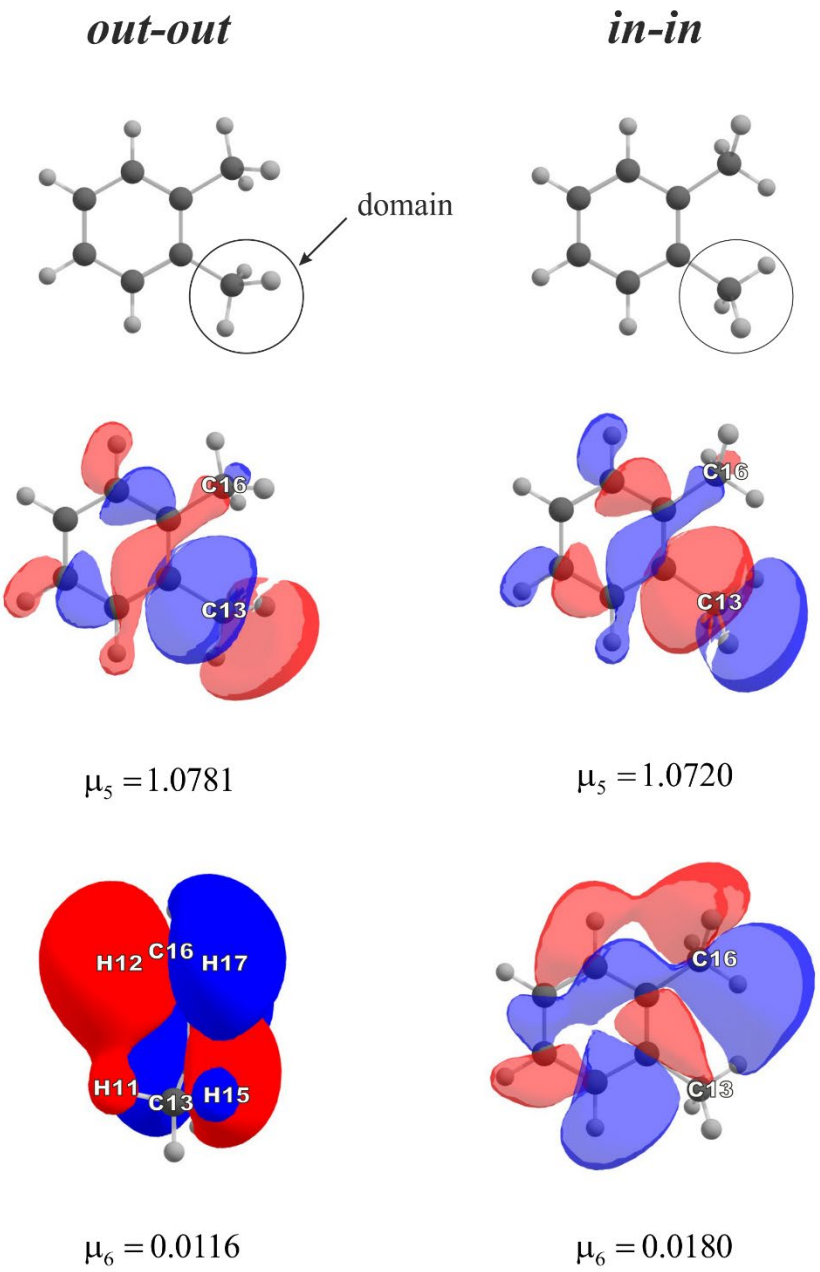

Fig 2.8. DAFH eigenvectors describing the methyl (domain) interaction with the remaining fragment together with their occupations.

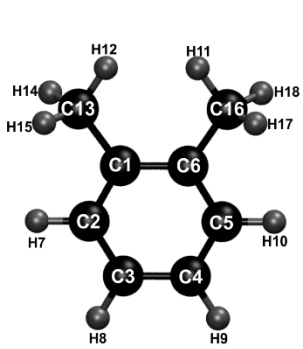

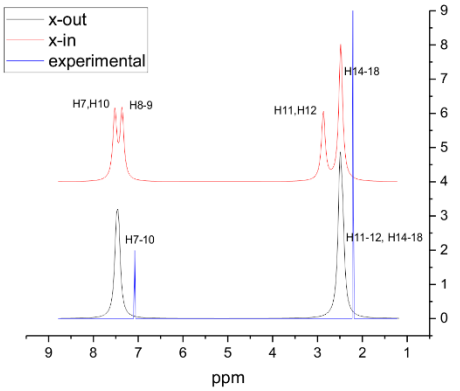

atom	in-in	out-out
H7	7.5264	7.4912
H8	7.3612	7.4371
H9	7.3620	7.4372
H10	7.5172	7.4830
H11	2.8700	2.4973
H12	2.8710	2.5008
H14	2.4816	2.4397
H15	2.4816	2.5007
H17	2.4824	2.4973
H18	2.4823	2.4399

Fig 2.9: Calculated ^{1}H NMR spectra of out-out (black line) and in-in (red line) xylene.

Tetramer of 8-hydroxyquinoline connected via hydrogen bonds

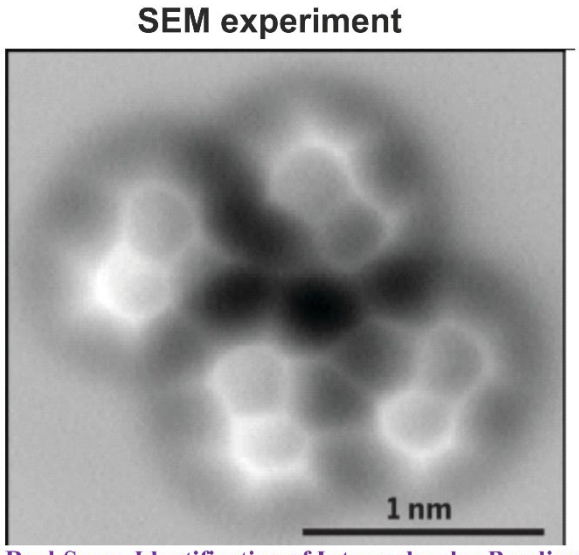

„Real-Space Identification of Intermolecular Bonding with Atomic Force Microscopy"
J. Zhang et al., Science, 2013, 342, 611-614 .

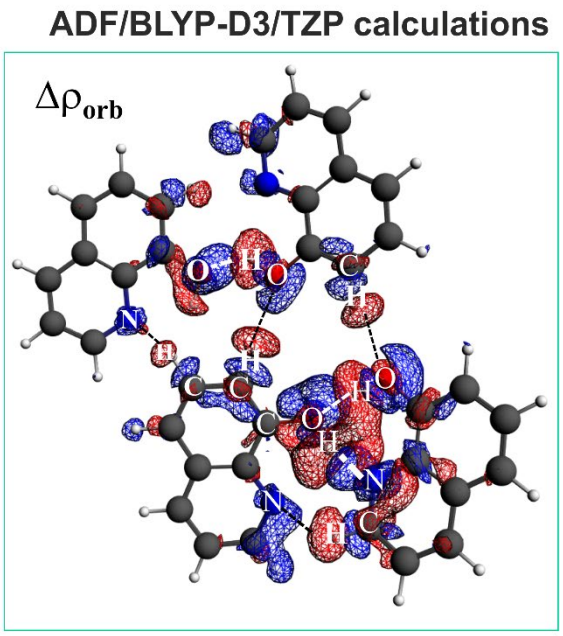

$\Delta\rho_{orb}=\rho_{molecule}-(\rho_1+\rho_2+\rho_3+\rho_4)^{ort}$

Fig 2.10: Calculated deformation density $\Delta\rho_{orb}$ from ADF/BLYP-D3/TZP (right) confronted with the observable experimental SEM image for hydrogen bonds connecting a tetramer of hydroxyquinoline. Red area of $\Delta\rho_{orb}$ shows outflow, whereas blue inflow of electron density due to formation of various hydrogen bonds – the calculated picture fits qualitatively well into the experimental SEM image (left). "Ort" abbreviations stems from orthogonalization.

Table 2.2. Calculated frequencies (cm^{-1}) from BLYP/TZP with the corresponding C–H distances (Å).

BLYP/TZP	$\nu(C–H_{in})$	$D(C–H_{in})$	$\nu(C–H_{out})$	$D(C–H_{out})$	Δd $D(C–H_{out})$- $D(C–H_{in})$	$\Delta\nu$ ν $(C–H_{out})$- ν $(C–H_{in})$
out–out	3013	1.1003	2964	1.1032	0.003	–49
in-in	3032	1.0968	2978	1.1025	0.006	–54

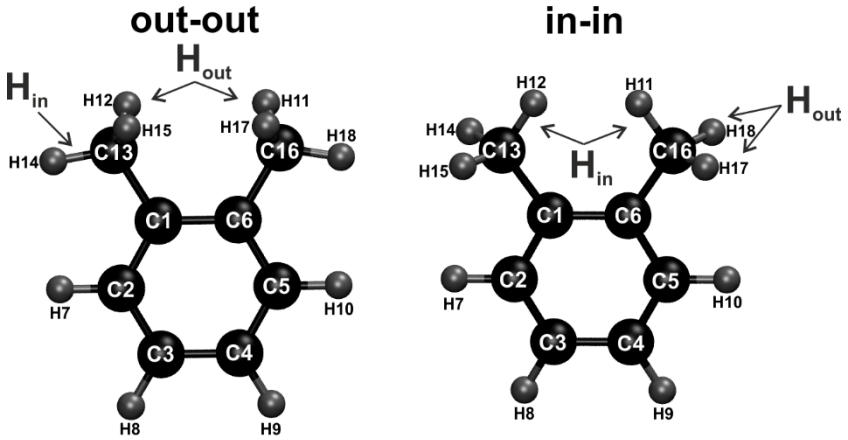

Fig 2.11: Designation of in-plane ($\mathbf{H_{in}}$) and out-of-plane ($\mathbf{H_{out}}$) hydrogen atoms of methyl groups.

PART 3 – EDDB aromaticity

The electron density of delocalized bonds (EDDB) facilitates quantitative analysis of different bond-conjugation patterns and provide a bird's-eye view on the global aromaticity and resonance effects in molecular systems that due to their size and complex structure have been the major challenge for other aromaticity descriptors.[1,2] The EDDB(r) function derives from the original method of the electron density (ED) partitioning that has been introduced to provide a uniform approach to quantify electron delocalization in molecular systems ED(r) = EDLA(r) + EDLB(r) + EDDB(r), where EDLA represents electrons localized on atoms (inner shells, lone pairs), EDLB represents electrons in Lewis-like localized bonds, and EDDB represents electrons delocalized between conjugated bonds (multicenter electron sharing, aromatic rings).[1,2] The latter component is of special interest in the context of aromatic stabilization effect, especially if one consider aromaticity as a property of the ground-state electron density in the spirit of the first Hohenberg-Kohn theorem of the conceptual density functional theory (DFT). Formally, the electron density of delocalized bonds is defined in the basis of natural atomic orbitals (NAO), $\mathrm{EDDB}(r) = \sum_{\mu,\nu} \chi_\mu^\dagger(r) D_{\mu\nu}^{\mathrm{DB}} \chi_\nu(r)$, where the corresponding DB-density matrix reads $\mathbf{D}^{\mathrm{DB}} = \frac{1}{2}\mathbf{P}\left[\sum_{\alpha,\beta\neq\alpha}^{\Omega} \mathbf{C}_{\alpha\beta}\boldsymbol{\varepsilon}_{\alpha\beta}\boldsymbol{\lambda}_{\alpha\beta}^2\mathbf{C}_{\alpha\beta}^\dagger\right]\mathbf{P}$. In the latter equation $\mathbf{P}$ represents the standard charge and bond-order matrix,[6] $\mathbf{C}_{\alpha\beta}$ is a matrix of linear-combination coefficients of the appropriately orthogonalized two-center bond-order orbitals (2cBO), $\boldsymbol{\lambda}_{\alpha\beta}$ stands for a diagonal matrix collecting the corresponding 2cBO occupation numbers, $\boldsymbol{\varepsilon}_{\alpha\beta}$ represents a diagonal matrix of the bond-conjugation factors, and $\boldsymbol{\Omega}$ denotes the system of conjugated bonds (it is by default a set of all the possible atomic pairs in a molecule).[1,2] The definition of $\boldsymbol{\varepsilon}_{\alpha\beta}$ involves a series of projections of localized 2cBO onto their three-center counterparts, followed by the projection onto the delocalized (in nature) occupied molecular orbitals (MO). Formal definition of this projection cascade is deeply rooted in the formalism of the orbital communication theory and as such it falls outside the framework of this short description. But it should be mentioned that the trace of the resulting DB-density matrix can be straightforwardly interpreted as the population of electrons delocalized through the system of conjugated bonds, $\boldsymbol{\Omega}$. EDDB is far more efficient than other electronic indices of aromaticity, especially in the case of highly accurate wavefunctions of large molecular systems.[1,2] For instance, calculation of the *kekulean* multicenter index (KMCI) takes from a dozen of seconds for 5- and 6-membered rings to several hours for the larger ones (up to 10 atoms), while the EDDB calculation takes about 1 s regardless of the ring size. Even the determination of global aromaticity/resonance effects in molecules contain hundreds of atoms is very fast; e.g., calculation of global EDDB(r) for the LEU-LYS-GLU-GLN-PROARG-HIS-PHE-TYR-TRP decapeptide (197 atoms) at the B3LYP/6-311G**//PM6 theory takes less than 40 s if the appropriate threshold for the 2cBO occupations is used and much less than 10 min otherwise.[1,2] Such speed-up is possible because within the EDDB formalism the multicenter electron sharing is approximated by means of decoupled three-atomic local resonances representing conjugations between the adjacent bonds only (cf. the Bridgeman-Empson method).[1,2]

Table 3.1. Aromaticity descriptors and their relative changes due to the corresponding rotations from out-out isomer.

Descriptor	*Out-Out*	*In-Out*	*In-In*	$\Delta_{\%In\text{-}Out}$	$\Delta_{\%In\text{-}In}$
HOMA	0.9687	0.9682	0.9597	-0.1	-0.9
$-NICS(1)_{zz}$	27.6990	26.9595	26.4016	-2.7	-4.7
EDDB	6.3732 0.9538 (σ) 5.4194 (π)	6.3339 0.9396 (σ) 5.3943 (π)	6.1972 0.9449 (σ) 5.2523 (π)	-0.6 -1.5 (σ) -0.5 (π)	-2.8 -0.9 (σ) -3.1 (π)

References

1. D. W. Szczepanik, M. Andrzejak, K. Dyduch, E. Żak, M. Makowski, G. Mazur and J. Mrozek, *Physical Chemistry Chemical Physics* 2014, **16**, 20514.

2. W. Szczepanik, *Computational and Theoretical Chemistry* 2016, **1080**, 33.

PART 4, FALDI – theoretical background and results

The Fragment, Atomic, Localized, Delocalized and Interatomic (FALDI) density decomposition scheme[1–5], built upon concepts from the Quantum Theory of Atoms in Molecules (QTAIM)[6] and the Domain Averaged Fermi Hole (DAFH)[7,8] approaches, decomposes the electron density at **r** into 1- and 2-centre contributions:

$$\rho(\mathbf{r}) = \sum_{\mathrm{A}}^{M} \mathcal{L}_{\mathrm{A}}(\mathbf{r}) + \sum_{\mathrm{A}}^{M-1} \sum_{B>A}^{M} \mathcal{D}_{\mathrm{A,B}}(\mathbf{r}) \tag{1}$$

where M is the number of nuclei. $\mathcal{L}_{\mathrm{A}}(\mathbf{r})$ provides the contribution at **r** of the density localized to atomic basin Ω_{A}, whereas $\mathcal{D}_{\mathrm{A,B}}(\mathbf{r})$ provides the contribution at **r** of the density delocalized simultaneously between atomic basins Ω_{A} and Ω_{B}. $\mathcal{L}_{\mathrm{A}}(\mathbf{r})$ and $\mathcal{D}_{\mathrm{A,B}}(\mathbf{r})$ are calculated by taking the product of all molecular orbital (MO) values at **r** with the overlap of MOs integrated over specific atomic basins (an atomic overlap matrix, or AOM). If an element of the AOM for atomic basin Ω_{A} is defined as

$$S_{ij}^{\mathrm{A}} = \sum_{ij}^{N} \int_{\mathrm{A}} \sqrt{\nu_i}\sqrt{\nu_j}\chi_i^*(\mathbf{r})\chi_j(\mathbf{r})d\mathbf{r} \tag{2}$$

where $\chi_i(\mathbf{r})$ is an MO with occupation $\sqrt{\nu_i}$, and the sum runs over all N MOs, then

$$\mathcal{L}_{\mathrm{A}}(\mathbf{r}) = \sum_{ij}^{N} \chi_i^*(\mathbf{r})\chi_j(\mathbf{r})(\mathbf{S}^{\mathrm{A}}\mathbf{S}^{\mathrm{A}})_{ji} \tag{3}$$

and

$$\mathcal{D}_{\mathrm{A,B}}(\mathbf{r}) = \sum_{ij}^{N} \chi_i^*(\mathbf{r})\chi_j(\mathbf{r})(\mathbf{S}^{\mathrm{A}}\mathbf{S}^{\mathrm{B}} + \mathbf{S}^{\mathrm{B}}\mathbf{S}^{\mathrm{A}})_{ji} \tag{4}$$

Note that the trace of the matrix product $\mathbf{S}^{\mathrm{A}}\mathbf{S}^{\mathrm{A}}$ is equal to λ(A), the QTAIM-defined localization index (LI) interpreted as the total number of electrons localized to a single atomic basin. Similarly, the trace of $\mathbf{S}^{\mathrm{A}}\mathbf{S}^{\mathrm{B}}$ + $\mathbf{S}^{\mathrm{B}}\mathbf{S}^{\mathrm{A}}$ is equal to δ(A,B), the QTAIM-defined delocalization index (DI) interpreted as the total number of electron pairs delocalized between two different atomic basins. Eqs. 3 and 4 are then the molecular-wide distributions of LI and DI, so that integrating $\mathcal{L}_{\mathrm{A}}(\mathbf{r})$ and $\mathcal{D}_{\mathrm{A,B}}(\mathbf{r})$ over all molecular space is equal to LI and DI, *i.e.* $\int_{\infty} \mathcal{L}_{\mathrm{A}}(\mathbf{r})d\mathbf{r} = \lambda(\mathrm{A})$. Furthermore, the QTAIM-defined atomic electron population for atom A, $N(\mathrm{A}) = \int_{\mathrm{A}} \rho(\mathbf{r})d\mathbf{r}$, is equal to the sum

of its LI and half of all associated DIs, $N(\mathrm{A}) = \lambda(\mathrm{A}) + \frac{1}{2}\sum \delta(\mathrm{A},\mathrm{X})$. The same holds true for FALDI, where the sum of an atom's localized and associated delocalized density contributions is equal to an *atomic* distribution,

$$\mathrm{g_A}(\mathbf{r}) = \mathcal{L}_\mathrm{A}(\mathbf{r}) + \sum_{\mathrm{B}\neq\mathrm{A}}^{M-1} \frac{1}{2}\mathcal{D}_{\mathrm{A,B}}(\mathbf{r}) \qquad (5)$$

and integrating the atomic distribution over all molecular space returns the QTAIM-defined atomic electron population, $\int_\infty \mathrm{g_A}(\mathbf{r})d\mathbf{r} = N(\mathrm{A})$. Therefore, FALDI is a natural and extremely useful tool to visualize the distribution, in real-space, of QTAIM-defined atomic and diatomic populations.

We have previously noted,[2] however, that the LIs defined by QTAIM does not describe electrons *exclusively* localized to a single basin and that these electrons can still be found in other basins as well. In order to visualize fully atom-localized electrons, we implemented[2] a procedure to calculate the overlap that localized electrons in a single basin have with all other electron distributions (de)localized on other basin or basin-pairs by comparing eigenvectors of $\mathbf{S}^\mathrm{A}\mathbf{S}^\mathrm{A}$ with eigenvectors of $\mathbf{S}^\mathrm{B}\mathbf{S}^\mathrm{B}$ as well as $\mathbf{S}^\mathrm{A}\mathbf{S}^\mathrm{B} + \mathbf{S}^\mathrm{B}\mathbf{S}^\mathrm{A}$. The procedure is known as the localized-delocalized overlap (LDO) adjustment and readers interested in an in-depth description and derivation can consult Ref. [2]. The resultant localized distribution, $\mathcal{L}''_A(\mathbf{r})$, is free of any LDO and describes electrons that can only be found, exclusively, in a single basin. In terms of chemistry, $\mathcal{L}''_A(\mathbf{r})$ therefore describes *core* electrons. Similarly, $\mathcal{D}''_{\mathrm{A,B}}(\mathbf{r})$ modified by the LDO adjustment describes both *valence* electrons and any partially delocalized *non-bonded* electrons, such as lone-pairs on amine groups. Note that we'll be dropping the double-primes from $\mathcal{L}''_A(\mathbf{r})$ and $\mathcal{D}''_{\mathrm{A,B}}(\mathbf{r})$ as all FALDI-based (de)localized electron counts and distributions in this work have been calculated using the LDO adjustment.

Finally, FALDI can be used to calculate deformation densities resulting from a conformational change from a reference conformer, *ref*, to a final conformer, *fin*.[1,5] To our knowledge, FALDI is the first scheme to be able to do so, whereas traditional deformation densities must be calculated from two or more entirely non-interacting reference states (usually resulting from molecular fragmentation). Conformational deformation density calculations are made possible by the decomposition in Eq. 1. Since the LDO-adjustment ensures that the terms in Eq. 1 are truly 1- and 2-centre terms, each localized and delocalized term can be separately transformed from the *fin* conformer to act as a suitable reference in the *ref* conformer. For instance, ${}^{fin}\mathcal{L}_\mathrm{A}(\mathbf{r})$ describing the core electron contribution at $\mathbf{r}$ in the *fin* conformer, can be compared to ${}^{ref}\mathcal{L}_\mathrm{A}(\mathbf{A_A r})$, where

$\mathbf{A}_\mathrm{A}$ is a transformation matrix relating the relative position and orientation of atom A in *fin* to its position and orientation in *ref*. The change in core density for atom A at $\mathbf{r}$ is then calculated by:

$$\Delta_c\mathcal{L}_\mathrm{A}(\mathbf{r}) = {}^{fin}\mathcal{L}_\mathrm{A}(\mathbf{r}) - {}^{ref}\mathcal{L}_\mathrm{A}(\mathbf{A}_\mathrm{A}\mathbf{r}) \tag{6}$$

Delocalized density contributions, $\mathcal{D}_{\mathrm{A,B}}(\mathbf{r})$, depends on the relative position and orientation of two atoms, and a single transformation matrix is not sufficient to relate $\mathbf{r}$ in *fin* to a suitable $\mathbf{r}$ in *ref*. To this end, we introduced[1] a linear scaling scheme to calculate a transformation from *fin* to *ref* for $\mathcal{D}_{\mathrm{A,B}}(\mathbf{r})$ distributions relying on two transformation matrices $\mathbf{A}_\mathrm{A}$ and $\mathbf{A}_\mathrm{B}$, which, in the interest of brevity, we will not discuss here. The resulting change in a specific diatomic delocalized density contribution is then:

$$\Delta_c\mathcal{D}_{\mathrm{A,B}}(\mathbf{r}) = {}^{fin}\mathcal{D}_{\mathrm{A,B}}(\mathbf{r}) - {}^{ref}\mathcal{D}^{\mathcal{R}}_{\mathrm{A,B}}(\mathbf{r}) \tag{7}$$

where ${}^{ref}\mathcal{D}^{\mathcal{R}}_{\mathrm{A,B}}(\mathbf{r})$ refers to the weighted contribution of ${}^{ref}\mathcal{D}_{\mathrm{A,B}}$ at both $\mathbf{A}_\mathrm{A}\mathbf{r}$ and $\mathbf{A}_\mathrm{B}\mathbf{r}$. Finally, the total conformational deformation density is then the sum of all localized and delocalized density changes,

$$\Delta_c\rho(\mathbf{r}) = \sum_{\mathrm{A}}^{M}\Delta_c\mathcal{L}_\mathrm{A}(\mathbf{r}) + \sum_{\mathrm{A}}^{M-1}\sum_{\mathrm{B>A}}^{M}\Delta_c\mathcal{D}_{\mathrm{A,B}}(\mathbf{r}) \tag{8}$$

and, barring numerical errors introduced through the use of AOMs, $\int_\infty \Delta_c\rho(\mathbf{r})\,d\mathbf{r} = 0$. Note that our in-house algorithm for calculating conformational deformation densities currently only allows for a single translational, rotational or scaling transformation. As such, we are presently still limited to calculating conformational deformation densities between two conformers that differ only along a single redundant coordinate, as opposed to two fully optimized conformers. However, conformational deformation densities between conformers separated by more than one redundant coordinate can be accurately calculated by successive applications of the algorithm.

Computational details

FALDI-based conformational deformation density calculations can presently only be calculated for a limited set of linear transformations. Due to this and in order to perform analyses on fully optimized products of transformations two methyl groups in optimized structures were rotated to generate input (initial) structures. For instance, for the *in-in* → *out-out* transformation, the methyl groups of the fully optimized *out-out* structure was rotated to generate a suitable input (*in-in*). The corresponding wavefunctions, calculated at B3LYP/6-311++G(d,p) level, were analysed using

AIMAll, ver. 16.10.31 and FALDI (in-house codes) in order to produce conformational deformation density data for each of the transformations.

FALDI – Brief theoretical background

Detailed results – FALDI

FALDI-based conformational deformation densities can provide a qualitative overview of the i) total, ii) molecular-wide atom-localised and (iii) interatomic delocalised density changes in 3D real-space upon a conformational change. In order to ease interpretation, we will analyse the data mostly in terms of two fragments: fragment *A*, consisting of the entire bay, including atoms C1 and C6 as well as the two methyl groups, and fragment *B*, consisting of the remainder of the aromatic ring (*i.e.* from C2 to C5, including H-atoms). The total conformational deformation density, $\Delta_c\rho(\mathbf{r})$, for the *out-out* → *in-in* change as well as for the *in-in* → *out-out* change is shown in Figure 4.1. The changes are mostly symmetrical, *i.e.* a charge increase at a given **r** in the *in-in* → *out-out* transformation is mirrored by a charge decrease in the *out-out* → *in-in* transformation, despite the geometrical constraints described in the Computational Details section.

From the $\Delta_c\rho(\mathbf{r})$ distribution in Figure 4.1, a clear increase in density between H11 and H12 is seen for *out-out* → *in-in*, whereas density is decreased in the same region for *in-in* → *out-out*. The increase in charge density between "clashing" H-atoms is in accordance with Feynman's theorem[1] of maximizing the attractive forces acting on nuclei, and the same property is observed with the formation of most bonds (whether weak, covalent or ionic). The loss of density between H-atoms of the methyl groups upon *in-in* → *out-out* shows that the density found in the internuclear region is considerably less in *out-out* than *in-in* (but does not mean that density isn't shared between H-atoms when *out-out* is analysed separately, as shown in the ETS-NOCV section). On the other hand, the aromatic ring appears to be losing electron density on *out-out* → *in-in*, specifically for fragment *B*, whilst gaining density in *in-in* → *out-out*.

Interestingly, Figure 4.1 is qualitatively quite similar to the IQA-defined additive atomic energy changes, as shown in ESI, Part 1, Figure 1.1 *(FAMSEC)*, and for the most part, we report a stabilization in additive atomic energy wherever an increase in density is observed. In particular, additive energy changes in ESI, Part 1, Figure 1.1 *(FAMSEC)* for the *in-in* conformer reveals that the carbon atoms of fragment *B*, for which a decrease in density takes place, are mainly destabilized on the *out-out* → *in-in* transformation. On the other hand, the increase in density between H11 and H12 (Figure 4.1) correlates perfectly well with the largest decrease in additive atomic energy (hence most significant stabilization) found for these two H-atoms. Furthermore, the largest depletion in density was computed for the methyl H-atoms *not* involved in the steric

contact in *in-in* and this phenomenon has been recovered perfectly by the increase in the additive atomic energies of these atoms, as shown in ESI, Part 1, Figure 1.1 (*FAMSEC*).

The integrated total deformation density values for fragments *A* and *B* are also shown in Figure 4.1. Fragment *A* lost 0.002 electrons on *out-out* → *in-in,* whereas fragment *B* gained 0.002 electrons – seemingly opposite of what is observed on the associated isosurfaces. This observation can be explained by further decomposing $\Delta_c\rho(\mathbf{r})$ to localized and delocalized contributions. The former tends to be densely packed around the nucleus and the latter diffusely spreads out between multiple atoms, making their relative contributions unclear at a single isovalue.

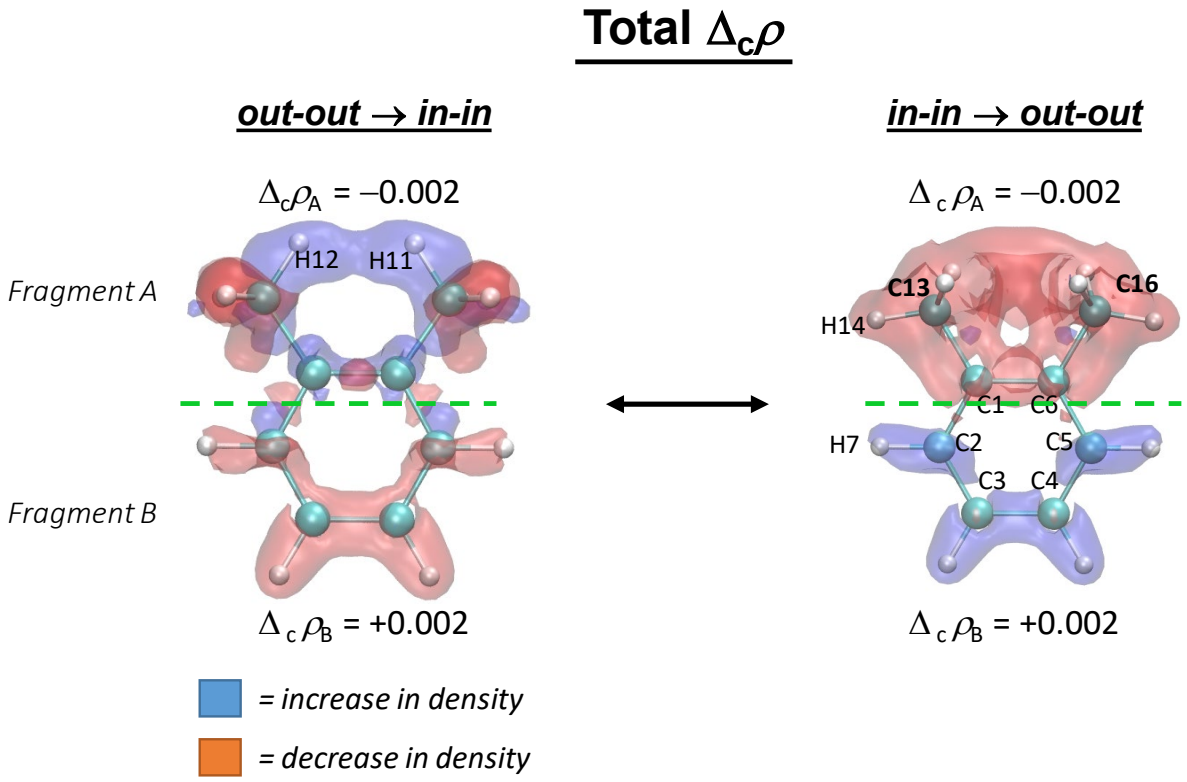

Figure 4.1. FALDI-based total conformational deformation density, $\Delta_c\rho(\mathbf{r})$, corresponding to *out-out* → *in-in* (left) and *in-in* → *out-out* (right). Isovalue = 0.0005 au.

Figure 4.2 shows the changes in FALDI-defined localized density, $\Delta_c\mathcal{L}(\mathbf{r})$, or atomic "core" density. Interestingly, the atoms of fragment *B* gain considerable localized density (+0.011 electrons) upon *out-out* → *in-in*, predominantly on C2/C5. A loss of localized density is observed for fragment *A* (–0.013 electrons), mostly centred on the methyl carbons C13/C16. Correspondingly, Figure 3 shows the changes in FALDI-defined delocalized density, $\Delta_c\mathcal{D}(\mathbf{r})$, or interatomic "valence" density: for *out-out* → *in-in*, a loss in delocalized density is seen in fragment *B* (–0.009 electrons), whereas a gain is observed in fragment *A* (+0.011 electrons, mostly between H-atoms involved in the steric contact). Note that $\Delta_c\rho = \Delta_c\mathcal{L} + \Delta_c\mathcal{D}$ and since for the entire

molecule $\Delta_c\rho = 0$, an overall 0.002 electrons are converted from localized to delocalized on *out-out* → *in-in*.

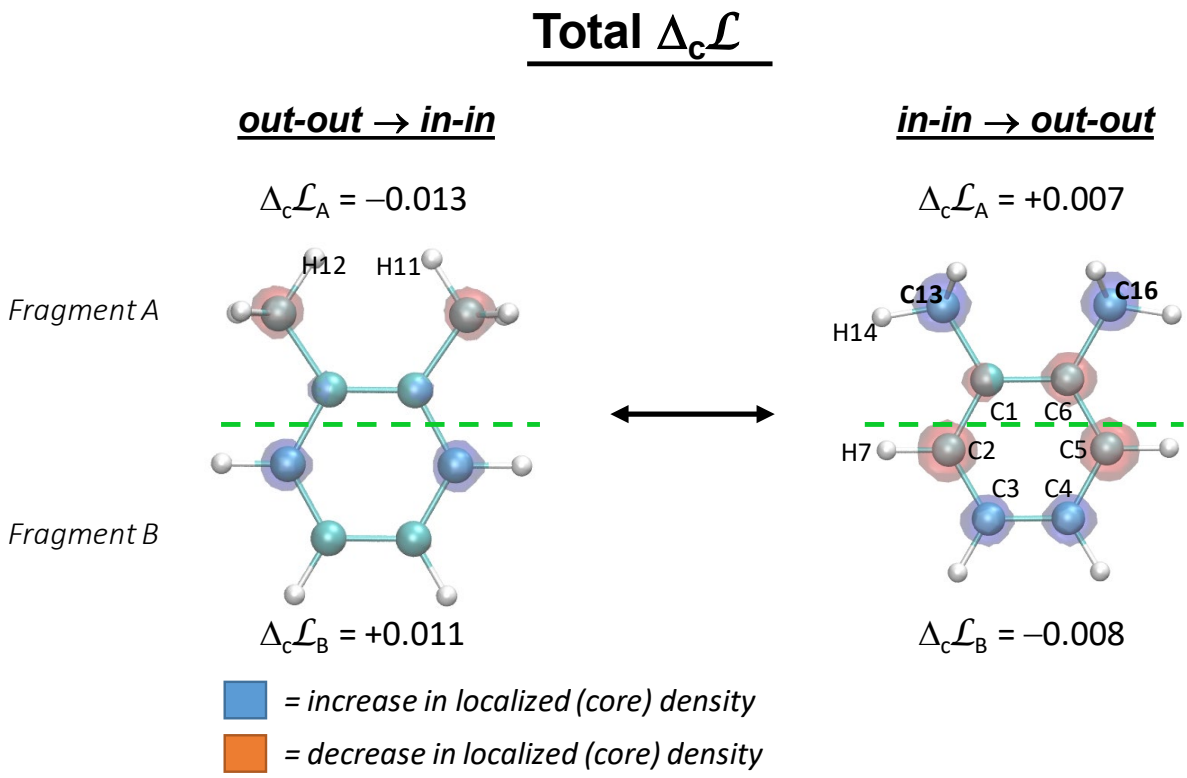

Figure 4.2. FALDI-based localized conformational deformation density, $\Delta_c\mathcal{L}(\mathbf{r})$, corresponding to *out-out* → *in-in* (left) and *in-in* → *out-out* (right). Isovalue = 0.0005 au

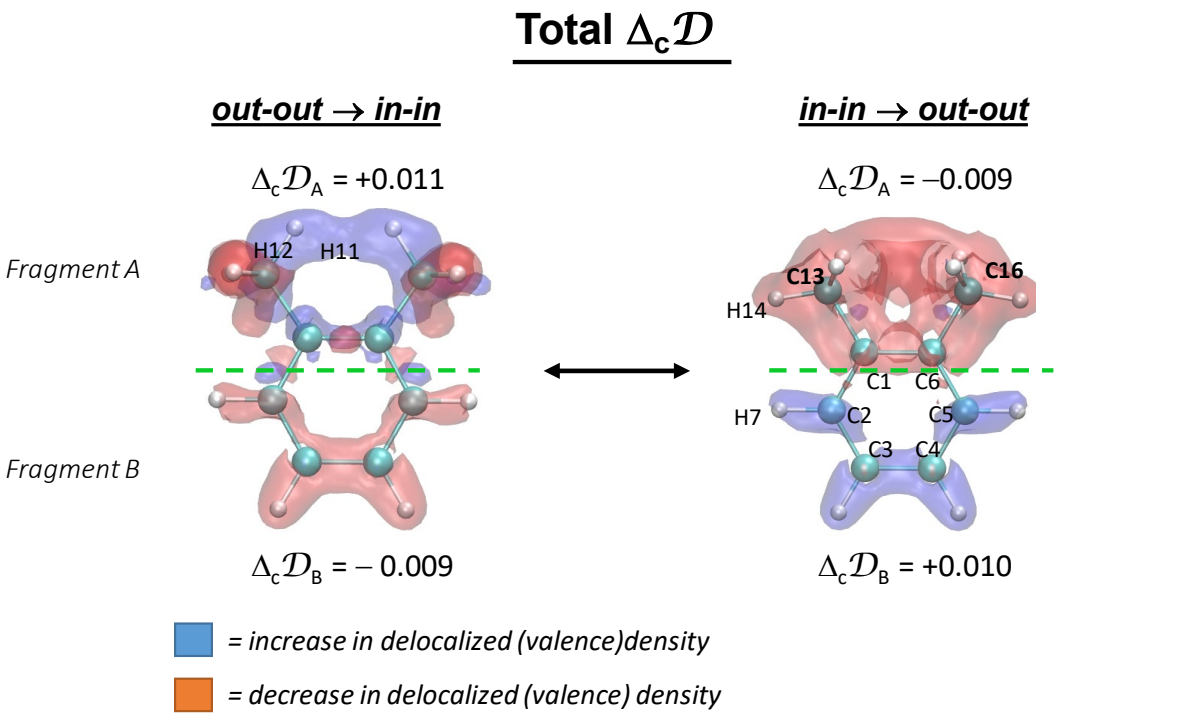

Figure 4.3. FALDI-based delocalized conformational deformation density, $\Delta_c\mathcal{D}(\mathbf{r})$, corresponding to *out-out* → *in-in* (left) and *in-in* → *out-out* (right). Isovalue = 0.0005 au

Table 4.1. Total FALDI population changes for various fragments

	out-out → *in-in*				
	$\Delta_c\rho$	$\Delta_c\mathcal{L}$	$\Delta_c\mathcal{D}$	$\Delta_c\mathcal{D}^{intra}$	$\Delta_c\mathcal{D}^{inter}$
Fragment *A* – *Bay*	–0.002	–0.013	+0.011	+0.131	–0.119
Fragment *B* – *Ring*	+0.002	+0.011	–0.009	+0.059	–0.068
Sum	*0.000*	*–0.002*	*+0.002*	*+0.190*	*–0.187*

	in-in → *out-out*				
	$\Delta_c\rho$	$\Delta_c\mathcal{L}$	$\Delta_c\mathcal{D}$	$\Delta_c\mathcal{D}^{intra}$	$\Delta_c\mathcal{D}^{inter}$
Fragment *A* – *Bay*	–0.002	+0.007	–0.009	–0.084	+0.075
Fragment *B* – *Ring*	+0.002	–0.008	+0.010	–0.049	+0.059
Sum	*0.000*	*–0.001*	*+0.001*	*–0.133*	*+0.134*

Figures 4.1 to 4.3 give a clear overview of the density changes within the molecule. However, in order to provide a quantitative picture of the interplay between localized and delocalized density changes, we have collected the total FALDI-based atomic electron populations for fragments *A* and *B* in Table 4.1. Table 4.1 also provides the decomposed total delocalized density change, $\Delta_c\mathcal{D}$, into density delocalized within atoms of a fragment, $\Delta_c\mathcal{D}^{intra}$, as well as density delocalized between remaining atoms of the other fragment, $\Delta_c\mathcal{D}^{inter}$. Atoms of both fragments share significantly more electrons amongst themselves upon *out-out* → *in-in* ($\Delta_c\mathcal{D}^{intra}$ = +0.131 and +0.059 electrons for fragments *A* and *B*, respectively), but each fragment experiences significantly fewer electrons delocalized with the other fragment ($\Delta_c\mathcal{D}^{inter}$ = –0.119 and –0.068 electrons for fragments *A* and *B*, respectively). In addition, fragments *A* and *B* lose (–0.013) and gain (+0.011) core electrons, respectively. The net effect of all localized and delocalized density changes is such that a small fraction of electrons (0.002) is transferred from the bay into fragment *B*. Trends opposite in sign are seen upon *in-in* → *out-out*: decreased intra-fragment delocalization for both fragments (–0.084 and –0.049 electrons for *A* and *B*, respectively) but increased inter-fragment delocalization (+0.075 and +0.059 electrons for *A* and *B*, respectively).

Putting the results from Figures 4.1 to 4.3 and Table 4.1 together, we can arrive at the following conclusions related to FALDI-based conformational deformation densities:

i. *out-out* → *in-in* leads to significantly increased intra-fragment delocalized density (a total of $\Delta_c\mathcal{D}^{intra}$= +0.190 electrons) but at the cost of inter-fragment delocalization (a total of $\Delta_c\mathcal{D}^{inter}$ = –0.187 electrons). This effect is twice as significant for fragment *A* than for fragment *B*.

ii. *in-in* → *out-out* leads to a significant loss of intra-fragment delocalized density (a total of $\Delta_c \mathcal{D}^{intra}$ = –0.133 electrons) but leads to increased inter-fragment delocalization (a total of $\Delta_c \mathcal{D}^{inter}$ = –0.187 electrons), to a similar degree on both fragments.

iii. Localized (core) electron changes are of the same magnitude, but opposite in sign, as changes in the net delocalized (valence) electron populations. For the *out-out* → *in-in* transformation a large increase in core electrons is observed for fragment *B* at the expense of a loss of valence electrons, whereas the opposite is observed in *in-in* → *out-out*.

iv. Fragment *B* gains a significant number of delocalized density upon *in-in* → *out-out* ($\Delta_c \mathcal{D}$ = +0.010 electrons), and correlates well with the increased resonance stabilization for *out-out* observed by EDDB analysis (part 3) measured for the aromatic ring. In addition, the source of the increased delocalized density for fragment *B* is from density shared with fragment *A* ($\Delta_c \mathcal{D}^{inter}$ = +0.059 electrons), and again corroborates the EDDB observation that the methyl groups contribute significantly to the resonance stabilization of the aromatic ring.

It is thus clear that both fragments experience increased resonance (in terms of delocalized density) on *out-out* → *in-in*, and we therefore expect these fragments to be *locally* stabilized. This finding is fully corroborated by FAMSEC, with *loc*-FAMSEC = –6.6 and –1.5 kcal·mol^{-1} for fragments *A* and *B*, respectively, on *out-out* → *in-in*. On the other hand, both fragments experience decreased inter-fragment resonance, and FAMSEC again shows that these fragments exhibit a destabilizing effect on the entire molecule (*mol*-FAMSEC = +1.5 and +3.8 kcal·mol^{-1} for fragments *A* and *B*, respectively, on *out-out* → *in-in*).

Considering that the total energy difference favours the *out-out* rather than the *in-in* conformer, it stands to reason that increased molecular-wide delocalization ($\Delta_c \mathcal{D}^{inter}$ = +0.134 electrons), as well as the increased involvement in resonance of core electrons ($\Delta_c \mathcal{L}$ = –0.001 electrons), in *out-out* is energetically more favourable than the more localized resonance observed in *in-in*. Our FALDI results also strengthen our hypotheses that i) the formation of an H···H clash in *in-in* is not responsible for the conformational energy difference, and rather leads to increased delocalization (and local stabilization) in the bay region, and ii) that the *out-out* conformer is more stable than *in-in* as a result of a molecular-wide stabilization in *out-out*, rather than increased local stabilization in *in-in*.

FALDI – Static density analysis of the *in-in* conformer

In order to gain insight with regards to the character and source of the density in the internuclear region between atoms H12 and H11 of the *in-in* conformer, FALDI-based cross-section analysis of the static density[3,4] was done along the vector shown in Figure 4.4(a).

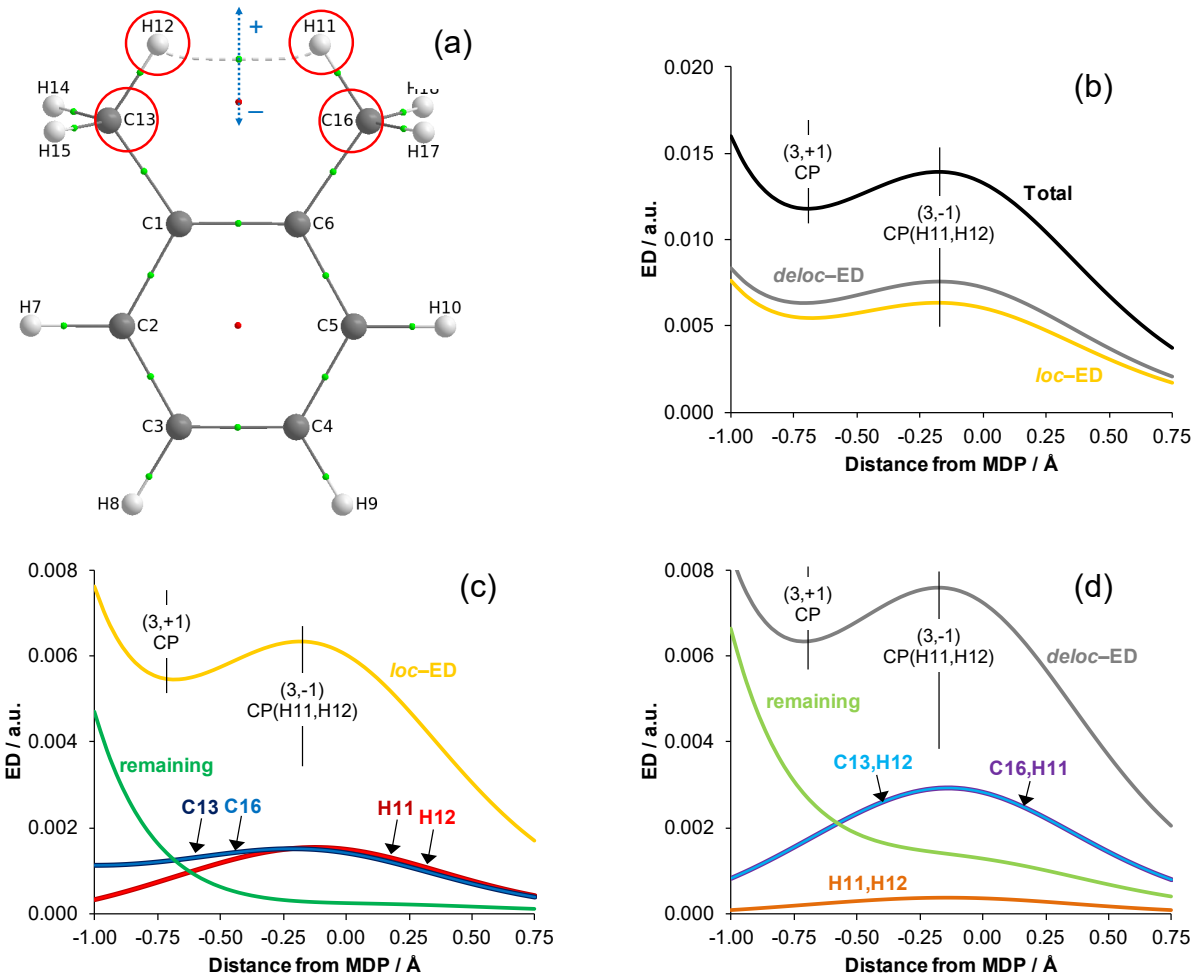

Figure 4.4. (a) Molecular graph of xylene conformer *in-in* and the vector followed for FALDI-based density decomposition analysis, (b) total density decomposition expressed in terms of total *loc*-ED and *deloc*-ED, (c) decomposition of *loc*-ED expressing major contributions and (d) decomposition of *deloc*-ED expressing major contributions.

The chosen vector passes through (i) the minimum density point (MDP, point of minimum density, along the vector, the λ_2–eigenvector, in the inter-nuclear region between H12 and H11), (ii) the QTAIM (3,-1) bond critical point on the atomic interaction line, also called a bond path, that links atoms H12 and H11, and (iii) the adjacent QTAIM (3,+1) ring critical point. Decomposition along this λ_2–eigenvector reveals (Figure 4.4(b)) that at the (3,-1) CP(H12,H11) and its close vicinity delocalised into the inter-nuclear region electron density, *deloc*-ED, dominates with 54.5%

contribution to the total ED (the localised electron density, *loc*-ED, constitutes 45.5% of the total ED – Table 4.2). The individual FALDI components contributing most to *loc*-ED are attributed mainly to four atoms (Figure 4.4(c)), namely C13, H12, H11 and C16, each atom contributing 24% to the *loc*-ED, Table 4.2. Importantly, about 81% of *deloc*-ED comes from the following atom-pairs: C13,H12 (38%), C16,H11 (38%) and H11,H12 (5%) – see Figure 4.4(d) and Table 4.2. Therefore, due to small contribution made by the H12,H11 atom-pair, it is more appropriate to refer to this interaction as CH···HC rather than H···H.

Table 4.2. Contributions made towards density at (3,-1) CP(H12,H11) of *in-in*.

Component	Density (a.u.)	% contribution
C13 *loc*-ED	0.00151	10.9
H12 *loc*-ED	0.00151	10.9
H11 *loc*-ED	0.00151	10.9
C16 *loc*-ED	0.00151	10.9
Total *loc*-ED	0.00632	45.5
H11,H12 *deloc*-ED	0.00036	2.6
C13,H12 *deloc*-ED	0.00290	20.8
C16,H11 *deloc*-ED	0.00290	20.8
Total *deloc*-ED	0.00758	54.5
Total density	0.01391	100.0

3D isosurfaces of these seven major components are shown in Figure 4.5, where it can be seen that (i) H12 and H11 share their density in a direct manner, forming a clear channel in the inter-nuclear region between each other and (ii) the density delocalised by the C13,H12 and C16,H11 spreads out well into the inter-nuclear H12---H11 region that is consistent with these atom-pairs most significant contribution made to the *deloc*-ED at the (3,-1) CP(H12,H11), hence also contributing to the formation of the AIL between H12 and H11.

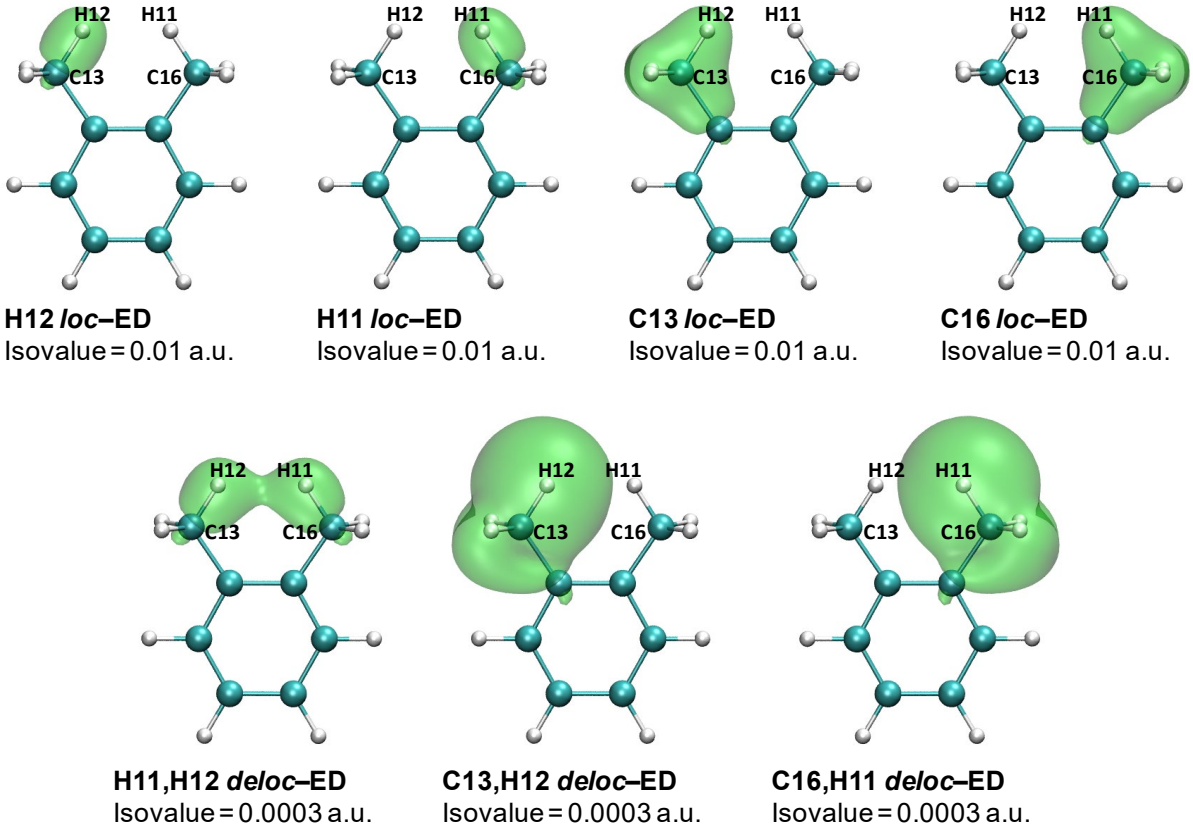

Figure 4.5. FALDI-based 3D isosurfaces of density distributions of the main contributors towards (3,-1) CP(H11,H12) presence.

References - FALDI Theoretical Background

1. J. H. Lange, I. Cukrowski, *J. Comp. Chem.* **2017**, *38*, 981–997.
2. J. H. de Lange, I. Cukrowski, *J. Comp. Chem.* **2018**, *39*, 1517–1530.
3. J. H. de Lange, D. M. E. van Niekerk, I. Cukrowski, *J. Comp. Chem.* **2018**, *39*, 2283–2299.
4. J. H. de Lange, D. M. E. van Niekerk, I. Cukrowski, *J. Comp. Chem* **2018**, *39*, 973–985.
5. I. Cukrowski, D. M. E. van Niekerk, J. H. de Lange, *Struct. Chem.* **2017**, *28*, 1429–1444.
6. R. F. W. Bader, In Atoms in molecules: A Quantum Theory; Oxford University Press: Oxford, **1990**.
7. R. Ponec, *J. Math. Chem.* **1997**, *21*, 323–333.
8. R. Ponec, *J. Math. Chem.* **1998**, *23*, 85–103.